HCAR1-dependent Effect of Therapeutic Lactate in Post-Stroke Pathophysiology in Mice

Karl Martin Frøseth Forbord

Master Thesis for the title of Master in Pharmacy

Department of Pharmaceutical Biosciences

School of Pharmacy

45 credits

The Faculty of Mathematics and Natural Sciences

UNIVERSITETET I OSLO

May 2019

HCAR1-dependent Effect of Therapeutic Lactate in Post-Stroke Pathophysiology in Mice

Karl Martin Frøseth Forbord

Master Thesis for the title of Master in Pharmacy

Department of Pharmaceutical Biosciences

School of Pharmacy

45 credits

The Faculty of Mathematics and Natural Sciences

UNIVERSITETET I OSLO

May 2019

2019

HCAR1-dependent Effect of Therapeutic Lactate in Post-Stroke Pathophysiology in Mice

Karl Martin Frøseth Forbord

Acknowledgements

Abstract

Cerebral stroke is the second leading cause of death worldwide and one of the most prevalent causes of long-term disability. The first priority in ischaemic stroke treatment is rapid recanalisation of the occluded artery, and the acute treatment arsenal was recently expanded by the advent of thrombectomy. However, even patients that receive successful recanalisation therapy may suffer from long-term neurological deficits and the available rehabilitating therapies are sparse. Development of neurorestorative treatments has broadly been stagnant.

There is mounting evidence for the importance of physical exercise in the prevention of primary and secondary stroke as well as stroke rehabilitation. The INTERSTROKE study listed physical inactivity as one of the five main risk factors for ischaemic stroke. The recently discovered hydroxycarboxylic acid receptor 1 (HCAR1) dependent enhancement of cerebral vascularisation by lactate may be a contributing factor to the reduced incidence and improved outcome seen in physically active populations.

The aim of the present study was to examine the possible neuroprotective effects of lactate by comparing neurological damage and microglia density in the affected tissue after induction of focal ischaemic stroke in the brains of HCAR1 knock-out and wild-type mice treated with lactate or saline. An HCAR1-dependent lesion-reducing effect of lactate was detected three weeks after permanent occlusion of the distal middle cerebral artery, but not after one week. The density of microglia in the penumbra was not significantly altered by lactate treatment in any genotypic group one week after induction stroke. These findings are indicative of an HCAR1-dependent neuroprotective effect of lactate that becomes significant between one and three weeks after stroke. Lactate and HCAR1-expression has no altering effect on the microglia density in the affected areas. These findings may contribute to the understanding of the rehabilitating effects of physical exercise in sub-acute stroke treatment.

x

Abbreviations

3,5-DHBA	3,5-dihydroxybenzoic
Ab	Antibody
ABC	Avidin-biotin complex
AD	Anoxic depolarisation
ADP	Adenosine diphosphate
AMPAR	α-amino-3-hydroxy-5-methyl-4-isoxazole-propionic receptor
ANLS	Astrocyte-neurone lactate shuttle
ASIC	Acid-sensing ion channel
ATP	Adenosine triphosphate
BBB	Blood-brain barrier
Bcl-2	B-cell lymphoma 2
Bcl-XL	B-cell lymphoma-extra large
BSA	Bovine serum albumin
cAMP	Cyclic adenosine monophosphate
CBF	Cerebral blood flow
CNS	Central nervous system
CPP	Cerebral perfusion pressure
CSF	Cerebrospinal fluid
CVR	Cerebral vascular resistance
Cyt C	Cytochrome C
DAB	3,3-diaminobezidine
DAMP	Danger associated molecular pattern
DAPI	4,6-diamidino-2-phenylindole
EC	Endothelial cell
ET	Endovascular therapy
ETC	Electron transport chain
Fab	Fragment antigen binding
Fc	Fragment crystallisable
GA	Glutaraldehyde
GDx	Glutathione peroxidase
GPCR	G Protein-coupled receptor
H&E	Haematoxylin and eosin

HCAR1	Hydroxycarboxylic acid receptor 1
HRP	Horseradish peroxidase
Iba1	Ionised calcium-binding adapter molecule 1
ICA	Internal carotid arteries
IHC	Immunohistochemistry
KO	Knock-out
MAb	Monoclonal antibody
MCA	Middle cerebral artery
MCAO	Middle cerebral artery occlusion
MCT	Monocarboxylate transporter
NaPi	Sodium phosphate
NCS	Newborn calf serum
NMDAR	N-methyl-D-aspartate receptor
NOX2	NADPH oxidase 2
NVU	Neurovascular unit
PAb	Polyclonal antibody
PARP-1	Poly (ADP-ribose) polymerase 1
PBS	Phosphate-buffered saline
PFA	Paraformaldehyde
PI3K	Phosphatidylinositol 3-kinase
PRR	Pattern recognition receptor
PSDP-95	Postsynaptic density protein 95
ROS	Reactive oxygen species
rt-PA	Recombinant tissue plasminogen activator
SOD	Superoxide dismutase
TCA	Tricarboxylic acid
TLR	Toll-like receptor
TUNEL labeling	Terminal deoxynucleotidyl transferase deoxyuride triphosphate nick and
VEGFA	Vascular endothelial growth factor A
wt	Wild-type

Table of contents

1 Introduction

1.1 Acute Ischaemic Cerebral stroke

1.1.1 Prevalence, Incidence and Mortality

Cerebral stroke is the second leading cause of death worldwide (1) and one of the most prevalent causes of long-term disability (2). According to the American Heart Association Stroke Statistics Committee; cerebral stroke ranked as No. 5 among all causes of death in the US in 2018 (3). An estimated 795 000 people in the US (0.24% of the population) experience a new or recurrent stroke each year (3). In 2010, stroke was ranked as No. 17 among deceases contributing to years lived with disability in the US (4). Approximately 3% of all men and 2% of all women reported that they were disabled because of stroke (Survey of Income and Program Participation) (5).

Between 1990 and 2010 the world experienced a considerable increase in the incidence of both ischaemic and haemorrhagic stroke (37% and 47% increase, respectively) and number of stroke associated deaths (21% and 20% increase, respectively) (2). During the same time period, the incidence and mortality were significantly reduced in high-income countries (Ischaemic: 13% and 37% respectively; haemorrhagic: 19% and 38% respectively). This is arguably due to the effects of an aging population, better and more readily available treatment options, combined with an incidence reduction among men and individuals over 65 years of age caused by advances in reduction of risk factors (6, 7).

1.1.2 Aetiology

Even though 87% of all cerebral strokes are ischaemic, and only 10% and 3% are intracerebral and subarachnoid haemorrhages respectively, the term cerebral stroke is used interchangeably (3). Distinctions are also made between global (affecting the entire brain) and focal strokes (affecting only a portion of the brain) (8). Acute ischaemic strokes are caused by an occlusion of a cerebral blood vessel, causing a permanent or transient stop in the supply of blood to the downstream brain tissue (8-10). In accordance with the TOAST (Trial of Org 10172 in Acute Stroke Treatment) classification, there are five subtypes of acute ischaemic stroke aetiologies: 1) large-artery atherosclerosis, 2) cardio embolism, 3) small-vessel occlusion, 4) stroke of other determined aetiology, and 5) stroke of undetermined aetiology (11). In an analysis of 5017 patient records in The German Stroke

Data Bank, cardio embolism was the most prevalent cause of ischaemic stroke, accounting for roughly one fourth of all cases, closely followed by large-artery atherosclerosis and small-vessel occlusion which made up one fifth each (12). Stroke of undetermined aetiology also made up approximately one fifth of the cases.

1.2 Physiology

1.2.1 Cerebrovascular physiology and regulatory mechanisms

The nervous tissue of the brain has a unique metabolic physiology compared to other tissues. With negligible amounts of intrinsic energy stores and a low tolerance for hypoxic conditions, the brain is in a constant need of supply from the circulatory system in order function properly. This is illustrated by the fact that the brain, which constitutes 2% of the human body mass, receives 15% of the cardiac output, 20% of the oxygen supply and 15% of the glucose supply (13, 14). The cerebral blood flow (CBF) is defined by the volume of blood flowing through a defined amount of brain tissue in a defined time (usually expressed as mL x $100g^{-1}$ x min^{-1}) (15). In healthy young adults the average whole-brain CBF is approximately 46 mL x $100g^{-1}$ x min^{-1}, but varies greatly between different structures in the brain and subregions of brain tissue (80 mL x $100g^{-1}$ x min^{-1} in grey matter and 20 mL x $100g^{-1}$ x min^{-1} in white matter in a resting state). As in other tissues, the blood flow is regulated by the perfusion pressure to the tissue and the vascular resistance in the tissue (in this case the cerebral perfusion pressure (CPP) and the cerebral vascular resistance (CVR):

$$CBF = \frac{CPP}{CVR}$$

CPP is dictated by the difference in cerebral arterial and venous pressure. CVR is controlled by a number of factors, including the viscosity of the blood, the capillary density, and the vessel diameter, the latter of which being the only factor involved in rapid physiological regulation of CBF under constant normal CPP, namely by regulation of the arteriole diameter. New insight indicates that contraction and dilation of pericytes on cerebral capillaries may be a major regulator of CBF (16).

During normal physiological conditions, the brain receives a surplus of oxygen and glucose. The brain extracts and metabolises only approximately one third of the oxygen, and one tenth

2

of the glucose delivered by the circulatory system (17). During an initial decrease in CBF, the brain will compensate by dilating the arterioles supplying the affected area (thereby decreasing the CVR). If the decrease in CBF intensifies, the oxygen extraction fraction may be doubled in order to maintain the cerebral oxygen metabolism.

Blood-brain barrier

The blood-brain barrier (BBB) is a multicellular vascular structure that tightly seals the milieu of the central nervous system (CNS) parenchyma from the fluctuating conditions of the blood (18, 19). The main anatomical constituent of the BBB is the ufenestrated endothelial cell (EC) layer with continuous intercellular tight junctions that allows for significantly low rates of paracellular transport (20). In addition, the ECs of the BBB exhibit very low rates of paracytosis, leaving the transport of molecules between the blood and the CNS parenchyma to a collection of highly specific transporters. The BBB ECs are part of a unique microenvironment that in recent years has been termed the neurovascular unit (NVU) (21). The NVU also includes the endothelial basal lamina, the parenchymal basal lamina, pericytes, and astrocytic endfeet; all of which contribute to the maintenance the physiological properties of the BBB through contact dependent and -independent signalling.

The role of lactate in CNS homeostasis and angiogenesis

For the remainder of the thesis, lactate refers to L-lactate, as it is the endogenous and physiologically active lactate enantiomer. The role of lactate in physiological CNS homeostasis is subject for several on-going debates. Through recent research, lactate has been associated with several favourable attributes in contrast to the preceding notion of lactate as a pathologic by-product of hypoxia (22). Accumulating evidence has given rice to the astrocyte-neuron lactate shuttle (ANLS) hypothesis (23). In short, the ANLS theory postulates that astrocytes extract glucose and produce lactate through glycolysis, which is shuttled to adjacent neurons where it is converted to pyruvate and utilized in the tricarboxylic acid (TCA) cycle to fuel the oxidative phosphorylation. For example; isolated neurons produce more CO_2 than astrocytes (24), neurons mitochondrial respiratory chain complexes are arranged in a way that promotes mitochondrial respiration, whereas astrocytes arrangement is suggestive of poor mitochondrial respiration (25), and high affinity monocarboxylate transporters (MCTs) are expressed in neurons whilst astrocytes express MCTs with lower affinity (26). It is important to underline that these proposals are not

entirely binary. Glucose also enters neurons and it is unlikely that ANLS operates at the same level in all neural populations.

Emerging evidence is also attributing lactate properties as a signalling molecule in the CNS. It has been indicated that lactate has effects on neuronal plasticity and memory (27), as well as a modulating effect on the excitability of specific populations of neurons (28, 29). The latter is in part mediated through the G protein-coupled receptor (GPCR) hydroxycarboxylic acid receptor 1 (HCAR1) previously known as GPR81 (29). After first being discovered (30), HCAR1 was shown to be selectively activated by lactate and to inhibit lipolysis in adipocytes through downregulation of cyclic adenosine monophosphate (cAMP) (31). HCAR1 was later detected in neuronal populations throughout the CNS (32), and found to have a significant presence in fibroblast in the perivascular space lining the pial blood vessels, as well as in a subset of pericytes in the intracerebral microvessels (33). Much like in adipocytes, lactate and the HCAR1 agonist 3,5-dihydroxybenzoic (3,5-DHBA) mediates dose dependent reduction of cAMP and downregulation of neuronal activity (recorded as Ca^{2+} spiking) through HCAR1 activation in several neuronal populations (33). Interestingly, lactate was found to mediate an increase in cAMP in the locus corerulus (34). This effect has been attributed to a receptor yet to be identified (34).

The discovery of angiogenesis, neurogenesis, and synaptic function being enhanced by vascular endothelial growth factor A (VEGFA) (35, 36), and the subsequent finding of an increase in VEGFA in the CNS in response to both endogenous and exogenous lactate (exercise and infusion) were indicative of a possible explanation for some of the neurological benefits of physical exercise. The mediating receptor was later determined to be HCAR1 (33). Current belief is that HCAR1 activation enhances VEGFA secretion through the phosphatidylinositol 3-kinase (PI3K)-Akt pathway in fibroblasts and pericytes, causing increased angiogenesis in the brain (33, 37), but this remains to be demonstrated directly. The parallel discovery that lactate potentiates wound healing (38) and mediates a neuroprotective effect in several ischaemic cerebral stroke models (39-41) led to the current hypotheses of HCAR1-lactate interaction being of importance for the outcome of ischaemic stroke.

Lactate is considered a volume transmitter, meaning it diffuses longer distances than the typical wiring transmitter (e.g. glutamate) (42). Depending on measuring method, in what brain region the measurement is made, and in what species, the baseline cerebral extracellular

4

lactate concentration ranges from 0.5 mM to 4.6 mM (for review, see Morland et al., 2015 (29)). Currently, the EC_{50} values of L-lactate acting on HCAR1 is believed to be in the range of 1-5 mM, which implies that HCAR1 is activated at L-lactate concentrations as low as 0.1 mM. Titrating lactate blood concentrations by intravenous infusion to reach 9.5 mM in freely moving rats demonstrated a 56 % increase in hippocampal extracellular lactate concentration (43). The indication of lactate in the blood entering the brain has been confirmed by measurement of arteriovenous differences in lactate concentrations after infusion and exercise (for review, see Morland et al., 2015 (29))

The innate immune system of the CNS
The CNS has until recent years been described as an "immune privileged" organ (44, 45). There has been a common conception of the CNS being an immunologically passive organ, and of the BBB as simply a barrier, sealing the CNS from the peripheral immune system. In recent decades, research has shown that the CNS possesses a highly specialised intrinsic innate immune system and that the BBB actively contribute to the immune responses of the CNS. The presence of pattern recognition receptors (PRRs) like the toll-like receptors (TLRs) on microglia, astrocytes, oligodendrocytes, endothelial cells and neurons indicates that CNS is equipped to recognise and respond by immune activation to pathological stimuli (46). The microglia cells have been recognised as the "powerhouse" of the CNS innate immune system. In their native state, the morphology of the microglia is characterised by a small cell body with long, thin processes, suited for sensing markers for tissue damage or infection (45, 47). When microglia are activated by danger associated molecular pattern (DAMP) - PPR interactions, transcriptional activation of proinflammatory genes occurs in a DAMP-specific manner. Such DAMPs may be exogenous, like lipopolysaccharides, or endogenous, like heat-shock proteins, extracellular adenosine triphosphate (ATP) and certain nucleic acid patterns. Two preliminary activated microglial phenotypes have been descried; the M1 (classical) phenotype, that has been deemed the pro-inflammatory phenotype and has been associated with increased neuronal death in several pathological states, and the M2 (alternative) phenotype that has been demonstrated to mediate anti-inflammatory processes (48, 49). In general, activated microglia acquire many macrophage-like characteristics, such as amoeboid morphology, phagocytosis, migratory capacity and major histocompatibility complex antigen presentation (50, 51). They also undergo rapid proliferation and migrate towards the source of DAMPs in order to increase in numbers.

Microglia originate from hematopoietic precursors from the yolk sac, making them the only cells in the CNS of hematopoietic origin. In contrast to other resident macrophages, like the Kuppfer cells of the liver, microglia are capable of self-replication and do not require recruitment from circulating monocytic precursors. Reestablishment of normal neuronal neurotransmitter release after various injury stimuli has been shown to counteract the inflammatory activity of microglia (52). The Ionised calcium-binding adapter molecule 1 (Iba1), an allograft inflammatory factor homologue, is an actin-binding protein expressed in the cytoplasm of microglia (53). It is considered an effective marker for microglia in brain sections from humans, mice and a number of other mammals (54). It is therefore often selected as the target antigen for immunohistochemical staining of microglia. Microglia originate from hematopoietic precursors from the yolk sac, making them the only cells in the CNS of hematopoietic origin.

In addition, larger arterioles penetrating the CNS parenchyma and post-capillary venules are lined with a perivascular space, a gap between the luminal endothelial basal lamina and the glial limitans (consisting of astrocyte end feet and parenchymal basal lamina) where cerebrospinal fluid (CSF) circulates. In these vessels the endothelial cell layer is permeable to certain circulating immune cells and allows for the presence of perivascular macrophages, mast cells and certain stains of T cells (21, 45, 55). This is also the case in other CSF-filled spaces like the leptomeningeal and ventricular spaces.

1.3 Pathophysiology

The high sensitivity of the brain to cessation of CBF is clearly encapsulated by the relationship between the duration of the stroke and the degree of damage to the brain and the patients loss of function (56). During a typical large vessel ischaemic stroke, 1.9 million neurons, 14 billion synapses and 12 kilometres of myelinated fibers are lost every minute (57).

If an occluded vessel results in a drop in CBF to the degree that the auto regulation of arteriole diameter and increase in oxygen extraction fraction is inadequate to supply the downstream tissue with sufficient amounts of oxygen, the result may be damage to the cells in the affected area. The volume of damaged tissue, and the severity of the damage is a result of multiple factors, including the duration and extent of the occlusion, the hypoxic sensitivity

of the affected area and the degree of collateral flow (15, 58). The area most heavily affected by the reduction on CBF is referred to as the ischaemic core and consists mainly of irreversibly damaged (necrotic) cells, whereas cells in adjacent areas that are exposed to a lesser decrease in CBF is referred to as the ischaemic penumbra. Cells in the ischaemic penumbra may be affected to the degree that synaptic activity seizes, but may be salvaged if the area is re-perfused within a short amount of time. CBF less than 10 mL x $100g^{-1}$ x min^{-1} usually lead to rapid necrosis in the affected area, whereas CBF between 10 and 20 mL x $100g^{-1}$ x min^{-1} may not be directly fatal if normal CBF is quickly re-established.

There are three main categories of cell death: apoptosis, necrosis and autophagy (59). Each category has characteristic morphological features and biochemical pathway, although the pathways may to a certain degree overlap. These biochemical processes may be activated by an injuring event (such as hypoxic insult), and are reversible until the process reaches a "point of no return" and the cell is considered dead. What this "point of no return" entails may vary, but cells are generally considered dead when one or more of the following criteria are met (as proposed by the Nomenclature Committee on Cell Death): 1) the integrity of the plasma membrane is lost, 2) the cell, including its nucleus, has undergone complete fragmentation into discrete bodies (apoptotic bodies), and/or 3) the dead cells (or its fragments) has been engulfed by a neighbouring cell. Apoptosis is a type of programed cell death (59, 60). Apoptosis is characterized by several morphological changes including a rounding-up and shrinking of the cell, retraction of pseaudopodes, nuclear fragmentation, blebbing of the plasma membrane (which remains intact until the final stages), and engulfment by resident phagocytes. Apoptosis characteristically cause no inflammation in the surrounding tissue. Caspases and B-cell lymphoma 2 (Bcl-2) family proteins are key regulators in apoptosis. Apoptosis can be initiated through an intrinsic or extrinsic pathway which activates different intracellular cascades (although at some points they overlap) (61). Necrosis is characterised morphologically by swelling of the cell and organelles leading to the rupture of the plasma membrane and subsequent spillage of the intracellular content, which stimulates inflammatory responses in adjacent tissues. (59). The notion that necrosis is merely an accidental consequence to unspecific stress is becoming increasingly out-dated as the evidence for necrosis being regulated by bio-chemical pathways is mounting and giving rise to the new term; necroptosis (62, 63).

1.3.1 Ischaemic and reperfusion phase

An ischaemic cerebral stroke can be divided in two phases: the ischaemic phase and the reperfusion phase. The ischaemic phase includes the events that may occur as a result of limited or no CBF to the affected area. The reperfusion phase includes the events that may occur as a result of reintroduced CBF to the affected area.

1.3.2 Ischaemic phase

The ischaemic phase is caused and characterised by the interrupted access to substrates from the circulatory system in the affected brain tissue, oxygen and glucose in particular (10, 64). As the energy metabolism is almost completely dependent on glycolysis and subsequent oxidative phosphorylation, a reduction or complete interruption of oxygen and glucose supply quickly leads to a decrease in cytosolic ATP concentration (c[ATP]). ATP-dependent processes tightly regulate neurons transmembrane ion gradients. Once ATP get sparse, the neurons no longer manage to maintain the ion homeostasis, which may result is a spreading depolarisation of neurons in the ischaemic area in a process referred to as anoxic depolarisation (AD) (65, 66). The depolarisation leads to opening of voltage-sensitive Ca^{2+}-channels and the cytosolic Ca^{2+}-concentration increases. The cytosolic Ca^{2+}-homeostasis is also dependent on ATP availability as the transport out of the cytosol (into the endoplasmatic reticulum or out of the cell) is mainly active (ATP-dependent). Increase in cytosolic Ca^{2+}-concentration (c[Ca^{2+}]) leads to Ca^{2+}-dependent neuronal exocytosis of vesicular pools of the excitatory amino acid neurotransmitter glutamate. In addition, the glutamate reuptake (to actrocytes and neurons) is also inhibited as a result of the ATP-depletion and transmembrane ion gradient discharge, leading to a significant increase in extracellular glutamate concentration. Inversion of the transmembrane ion gradient may also reverse the direction of glutamate transporters adding to the glutamate efflux (67).

The term "exotoxicity" refers to conditions where supra physiologic extracellular concentrations of glutamate cause cell death by activating ionotropic receptors, such as the N-methyl-D-aspartate receptors (NMDARs), the α-amino-3-hydroxy-5-methyl-4-isoxazole-propionic receptors (AMPARs), and kainate receptors, causing intracellular Ca^{2+} overload and activation of cell death pathways (64). Ca^{2+} serves a key role in neuronal physiology, not only as a cation in electrochemical signalling, but as an initiator and regulator of several

cellular functions. This is also true for the pathophysiology of ischaemic stroke. As the $c[Ca^{2+}]$ reaches pathologic levels, several pro-death pathways are activated (64).

The hypoxia-induced inhibition of oxidative phosphorylation also leads to accumulation of unutilized pyruvate from the glycolysis that ferments to lactate. Lactate accumulation, together with protons as a product of ATP hydrolysis leads to a pH decrease in the ischaemic areas, typically to between 6.5 to 6.0 or even lower depending on the severity of the ischaemic insult (68). Several subtypes of the acid-sensing ion channels (ASICs), members of the epithelial sodium channel superfamily, are widely expressed in CNS neurons. They are primarily Na^+-permeable, but the ASIC1a subunit has been shown to be Ca^{2+}-permeable as well (69, 70). When the pH decreases, protons bind to the ASICs extracellular region, opening the channels, which allow flux of cations. This contributes to the extensive depolarisation and Ca^{2+} overload in the ischaemic area.

1.3.3 Reperfusion phase

Free radicals and oxidative stress

Free radicals are produced even at physiological conditions, mainly as a by-product of oxidative phosphorylation by the mitochondria. The electron transport chain (ETC) "leaks" superoxide (O_2^-) to the intermembrane space and the mitochondrial matrix, but it is efficiently converted to hydrogen peroxide (H_2O_2) by superoxide dismutases (SODs), and is subsequently converted to water and oxygen by glutathione peroxidase (GDx) (71, 72). These enzymes are part of the cell´s enzymatic defence against free radicals, which together with molecular antioxidants renders physiological free radical production harmless to the neurons.

The term oxidative stress refers to conditions in which the neurons are exposed to excessive amounts of O_2 and reactive oxygen species (ROS) (73). Although free radicals are produced to a certain extent during the ischaemic phase, ROS are produced to a far greater extent during the reperfusion phase when O_2 is reintroduced to the tissue, as the rate of ROS production in part is dependent on the availability of O_2 and the activity of antioxidant enzymes (73, 74). One source of ROS overproduction during reintroduction of O_2 is the ETC of the mitochondria. Accumulated adenosine diphosphate (ADP) and O_2 availability provokes enhanced ETC activity, which in itself would increase the ROS production. In addition, elevated $c[Ca^{2+}]$ may inhibit ETC-complexes involved in the reduction or oxidation

of the electron-transport molecule ubiquinone. Normally, ubiquinone is reduced in a two-step reduction, first to semiquinone, and subsequently to a diol by ETC-complex I or II, before delivering the two electrons at complex III. Impairment of the efficiency of this transfer causes leakage of free semiquinone that may interact with O_2 to form O_2^- (74, 75). There are also several other contributors of ROS production like nicotinamide adenine dinucleotide phosphate (NADPH) oxidase 2 (NOX2), which has been associated with O_2^- production stimulated by NR2B-subunit containing NMDAR activity (76).

ROS overproduction causes cell death through a wide arsenal of mechanisms (73-75). A key pathway is through DNA damage. ROS-induced DNA damage causes over activation of poly (ADP-ribose) polymerase 1 (PARP-1), an abundant nuclear enzyme, which in turn promotes AIF release from mitochondria, and activation of p53 and nuclear factor κB (NF- κB), all of which are key promoters of cell death. ROS also cause lipid peroxidation and protein denaturation, which stimulates more ROS production and cellular damage in a vicious cycle.

Post-ischaemic immunosuppression
Infections are an unintuitive, yet leading cause of death in patients suffering from acute CNS injury (77). The term "central nervous system injury-induced immune deficiency syndrome" refers to a characteristic systemic suppression of cell-mediated immune responses following acute injury to the CNS. Between 16-23% of stroke victims suffer a secondary infection, pneumonia and urinary tract infections being most common. The immuosupression may be mediated through the hypothalamo-pituitary-adrenal axis, the sympathetic and parasympathetic nervous system.

Oedema and swelling
Ischaemic and post-ischaemic events lead to the disruption BBB integrity. The inability to retain circulating solvents may result in ionic and vasogenic oedema as well as secondary haemorrhage (78). Oedema in the reperfused area causes swelling, which may impose mechanical pressure on surrounding tissues, increasing intracranial pressure and causing adjacent secondary ischaemia if the tissue pressure exceeds capillary pressure.

Post stroke angiogenesis
An increase in angiogenesis in the adult rodent and human brain has been documented during certain pathophysiological conditions (79). The multi-step process of angiogenesis involves

endothelial cell proliferation and migration, branching, tube formation and anastomosis, all of which is stimulated by VEGF (80). In the penumbra of human stroke patients, angiogenesis develops within three to four days, where as in rodents the process has been observed after two days (81). In humans, serum VEGF concentrations are increased seven days after an ischaemic stroke and remain high for at least 14 days (82). Similar elevations of VEGF has been detected in rodent ischaemic brain tissue (83).

1.3.4 Neuroinflammation in stroke

Stroke associated inflammation is generally considered a post-ischaemic event, even though the inflammatory processes are initiated shortly after the arterial occlusion occurs (50). The coagulation cascade is triggered and activates compliments, platelets and ECs, which in turn traps leukocytes and causes microvascular occlusions (84). Adhesion molecules are transferred to the luminal surface of the vascular ECs and the production of proinflammatory signalling molecules is initiated (85). Paracelluar passage through the BBB is enhanced by the downregulation of junctional proteins in combination with proteases excreted by vascular leukocytes (19). Ischaemic insult and reperfusion also cause perivascular macrophage activation and mast cell degranulation. The resulting release of vasoactive and proinflammatory mediators such as histamine, proteases and cytokines promotes enhanced BBB permeability by increasing the expression of endothelial adhesion molecules, dilating the vessels and breaking down endothelial junctional proteins.

Membrane damage and depolarisation of neurons and glia cause release of ATP to the extracellular fluid of the brain parenchyma (86). ATP-PRR interaction causes microglia activation and proinflammatory cytokine release (21). Thus, extracellular ATP is an important initiator of early ischaemic inflammation. If the ischaemic conditions persist, the array of signalling molecules present in the parenchyma will change as a result of cells beginning to die. Markers for necrosis like extracellular nucleotides and products of leaked lytic enzymes are recognized by PRRs on microglia, endothelial cells, and perivascular macrophages as DAMPs, which enhances pro-inflammatory signalling and expression of adhesion molecules. Neuronal cell death cause cessation of cell-to-cell contact between neurons and microglia, which also enhances microglial activation (87). The spreading proinflammatory and immunosuppressive changes in the CNS parenchyma are the driving

force of ischaemic inflammation, setting the stage for the subsequent post-ischaemic inflammation.

Following the initiating inflammatory changes of the ischaemic phase, reperfusion is accompanied by post-ischaemic inflammation characterized by an orchestrated recruitment of various blood-borne leukocytes and lymphocytes. Although the concrete roles of the different immune cells in post-ischaemic inflammation remains to be fully understood, emerging evidence is linking certain outcomes to specific immune cells. In particular, the adaptive immune system has gained increased interest during the last decade. Lymphocyte deficient mice are protected in models of focal ischaemia (88) which might be attributed to a reduction of cytotoxic T-cells (89). Inhibition of adhesion molecules responsible for leukocyte recruitment has also been associated with reduced infarct volume in stroke models (90). In addition, the inflammation is enhanced by other characteristic events of the reperfusion phase, like ROS-overproduction.

It is important to note that the immune response also serves an important beneficial function, as it clears dead cells and necrotic debris after the stroke, laying the foundation for the subsequent structural and functional reorganization of the affected area. Microglia, accompanied by haematogenous macrophages, carry out the majority of the phagocytic "clean up" in a process coordinated by "find me" (attracting phagocytes to the injured cells) and "eat me" signals (inducing phagocytosis) (91, 92). In addition, selective elimination of microglia and macrophages in mice has been shown to exacerbate the ischaemic injury (93). Regulatory T-cells have been shown to appear after the acute phase and mediate neuroprotecive effects by down-regulating post-ischaemic inflammation through IL-10 secretion (94). These are some of the effects that highlight the complexity and duality of post-ischaemic inflammation.

1.4 Treatment

As discussed, time is of essence in the treatment of cerebral ischaemic stroke (56, 57). Naturally, the first priority is to reopen the occluded artery to reintroduce CBF to the affected area. After showing a beneficial effect 3 months after stroke (95), alteplase, an intravenous recombinant tissue plasminogen activator (rt-PA) was marketed world wide in 1995 for the treatment of stroke in a 3-hour time window from symptom onset. Subsequent studies have

shown benefits for patients treated up to 6 hours after onset of symptoms, although best results were achieved with patients treated within 3 hours (96). Inactive endogenous plasminogen will bind to fibrin and fibrinogen during the formation of a thrombus (97). t-PA cleaves plasminogen to active plasmin which dissolves the thrombus by cleaving fibrin and fibrinogen to fibrin and fibrinogen degradation products. After the thrombus is dissolved, plasmin is rapidly bound to its inhibitor α_2-antiplasmin and is thereby inactivated. There are several strict contraindications to the use of rt-PA (and similar fibrinolytic analogues) in clinical settings as the risk of intracranial haemorrhage is well documented (98). An abbreviated summary includes: malignant hypertension, recent trauma or surgery, pregnancy or parturition and history of previous intracranial haemorrhage. An alternative to systemic acute thrombolytic treatment has emerged during the last couple of years (99). Endovascular therapy (ET), of mechanical thrombectomy, has gained favour as an effective treatment modality in patients meeting certain indication criteria. The procedure is performed by catheterisation through femoral artery puncture (100). The catheter is guided through the internal carotid artery to the site of the large artery occlusion. A stent retriever, inserted through the catheter, removes the clot and re-establishes CBF to the ischaemic tissue. ET has demonstrated favourable functional outcome compared to patients receiving thrombolysis in pooled, individual-patient meta-analysis (99).

Although effective reperfusion therapies are available, there are limitations to the treatments. The short time window is currently the most limiting factor. Even with successful recanalisation, the majority of patients still suffer from neurological deficits (98, 101). Efforts to provide pharmacological therapeutic options for the recovery phase of ischaemic stroke are still mainly in preclinical stages of development (102). The main focus of these efforts is enhancement of neuroprotection, neurogenesis, and cerebral angiogenesis. The observation of stroke induced enhancement of neuroblast production from neuronal stem cells in the subventricular zone, and subsequent migration and maturation in the ischaemic penumbra gave hope for a new viable neurorestorative therapeutic target (103). The subsequent discovery of adult neuroblast proliferation and migration being stimulated through the PI3K-Akt signalling pathway (104) led to the search for a pharmacological or cell-based therapeutic that may drive functional improvement during recovery.

Several studies have demonstrated a significant correlation between survival time and the number of cerebral blood vessels in the cortical rim after ischaemic stroke (102). Therefore,

efforts are made to pharmacologically increase the vascular density of the brain parenchyma, before and after an ischaemic stroke. In experimental rodent models, drugs such as statins and phosphodiesterase 5 inhibitors enhance angiogenesis in the ischaemic border by increasing the expression of VEGF (105). Although some treatment strategies have moved on to clinical trials, the translation to clinical practice has to a large extent failed.

1.5   Modelling stroke in mice

The lack of *in vitro* models capable of modelling the complex pathophysiology of a focal ischaemic stroke makes the use of animal models necessary in stroke research. The majority ischaemic stroke models in use are designed to produce an occlusion in the middle cerebral artery (MCA) (MCAO) as the majority of human focal ischaemic stroke lesions appear with the equivalent size in the equivalent region of the cerebrum (106, 107). The MCA is one of the two terminal branches of the internal carotid arteries (ICA) (108). The ICA originates from the common carotid arteries at the level of the inferior border of the thyroid gland and divides into the MCA and the anterior cerebral artery in the Circle of Willis at the base of the brain. From there the MCA runs laterally and rostrally over the olfactory cortex where the lenticulostriate arteries branches of to supply both cortical and subcortical structures before it ends in a variable pattern of rostral, medial and caudal vessels.

There are several established models for MCAO, which may be categorised based on the location and duration of the occlusion (for review, see Carmichael, 2005 (107) and Canazza et al., 2014 (109)). The models where MCAO is induced proximal to the lenticulostriate arteries generaly result in ischaemic insult the striatum, hippocampus, thalamus, and overlaying parts of the cortex. Models where the occlusion is indused distal to the lenticulostriate arteries result in a more restricted ischemic insult to medial parts of the cortex (barrel cortex). The occlusion is ether induced permanently or transiently. Transient occlusions are often induced by the intra-luminal suture model. A surgical filament is introduced through the ICA to the base of the MCA. The suture may be permanent, but is often removed after a specific amount of time in order to reperfuse the downstream tissue. In the thromboembolic stroke model, purified thrombin is injected in the MCA resulting in infarcts in various locations of the hemisphere. The stroke is often made transient by administration of thrombolytic agents. Permanent occlusion may be achieved by

14

electrocoagulation, which requires surgical opening of the cranium before the MCA is occluded by using diathermic forceps. Permanent occlusion is also induced by embolic methods, commonly by inserting a macrosphere (300-400 μm in diameter) in to the ICA, which is lodged in the MCA producing infarcts similar to the intra-luminal suture model. Introduction of a microspheres (50 μm in diameter) in the MCA produce smaller, multifocal infarcts throughout the brain.

2 Aims of the study

There is mounting evidence indicating neuroprotective effects of lactate in the treatment of ischaemic cerebral stroke (39-41). In light of the newly discovered link between HCAR1, lactate, and vascularisation of brain tissue, the idea that HCAR1 expression and opportune lactate exposure is beneficial for the outcome of stroke by increasing collateral flow is a natural hypothesis. In addition, lactate has been demonstrated to have a modulating effect on several inflammatory processes (110-112). As inflammation plays a considerable role in the pathophysiology of cerebral ischemic stroke, examination of the influence of lactate and HCAR1 on post-stroke neuroinflammation is also a logical addition. The aim of the present study was to address the following questions:

1) How does lactate-mediated HCAR1-signalling influence the volume of stroke lesion caused by permanent distal middle cerebral artery occlusion?
2) How does lactate and HCAR1 influence the lesion development over time?
3) How does lactate and HCAR1 influence the microglia recruitment and proliferation in the affected tissues after focal ischaemic stroke?

3 Methods and materials

3.1 Animals

Animals included in this study were treated in strict accordance with national and regional ethical guidelines. All care and experiments were performed by Federation of Laboratory Animal Science Association (FELASA) certified personnel and approved by the Animal Use and Care Committee of the Institute of Basic Medical Sciences, The Faculty of Medicine, University of Oslo, and by the Norwegian Animal Research Authority (FOTS ID 14204; 12521). The mice strand originated from the Texas Institute of Genomic Medicine (Huston, TX) and was a kind gift from Prof. Stephan Offermanns (Max-Planck-institute, Bad Nauheim, Germany). The HCAR1 KO mice were generated as described by Ahmed et al. (113). In short, the exon encoding murine HCAR1 was replaced by a gene cassette encoding β-galactosidase (LacZ) and neomycin resistance by homologous recombination in embryonic stem cells. The line was back-crossed nine times with C57/Bl6-N mice after arriving in our laboratory and bred to homozygosis.

At the time of the occlusion operation, the mice were all 3 months ($\pm$ 2 weeks) of age. The mice were kept in groups up to five separated by gender in GreenLine cages. Some males were moved to separate cages due to aggressive behaviour. The mice were stalled in a 12 hour light /dark cycle and had food and water access *ad libitum*. All experiments were performed during the light part of the cycle.

3.1.1 Treatment groups

Wild-type and HCAR1 KO mice were randomly placed in two groups main groups: one was to be analysed one week after stroke, the other three weeks after stroke. Each main group consisted of two sub groups: one group was treated with intraperitoneal (i.p.) sodium L-lactate injections (the physiologic enantiomer of lactate, $\geq$ 99.0%, Aldrich, 71718, dissolved in 0.9% saline; pH-adjusted to 7.4), 2 g/kg, 24 and 48 hours after the occlusion operation. The control group received the same volume (per kg bodyweight) of 0.9 % saline.
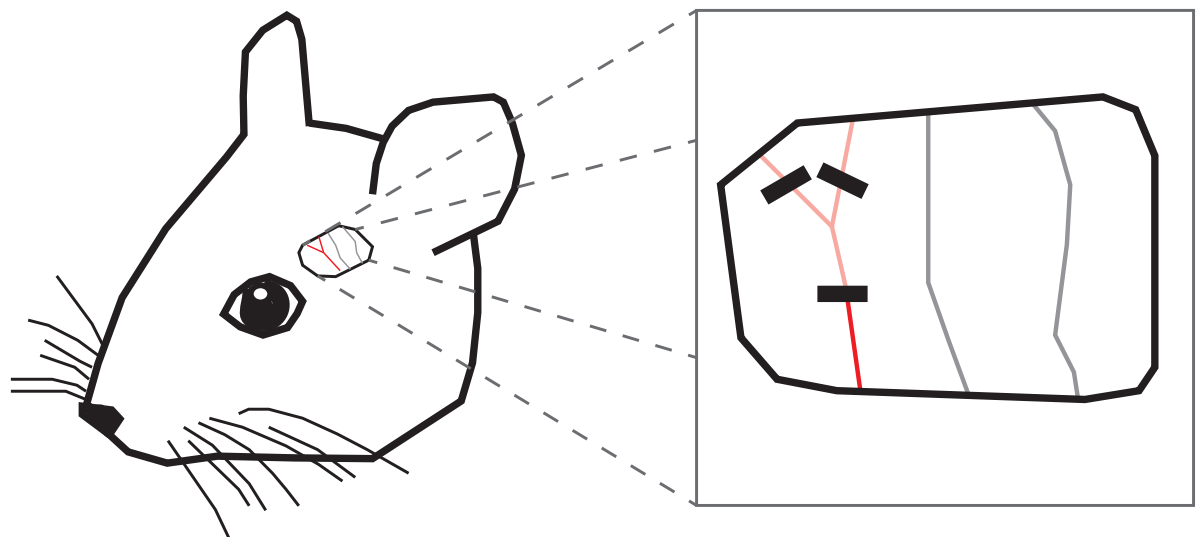
3.2 Permanent electrocoagulation of the distal middle cerebral artery

Procedure

The mice were individually placed in an induction chamber and anesthetized with 4% isofluorane (~70% N_2O, 30% O_2 + isofluorane). When sedated, they were injected intraperitoneally (i.p.) with an analgesic solution (buprenorphine/Temgesic 0.1 mg/kg, Indivior) and placed on a heat base set to 37 °C with the nose placed into a mask for anaesthesia. The isoflurane flow rate through the mask was initially kept at 4% until a surgical plane of anaesthesia was ensured (the animal was pinched between to toes, and this did not lead to any aversive movements of reflexes). The isoflurane flow rate was adjusted to ~1.5% for the remaining of the operation. Dexpanthenol eye ointment (Simplex eye ointment, Ophta) was applied to both eyes to keep them hydrated during the time in anaesthesia.

After the mice had been anaesthetized the area between the eye and the ear on the left side of the head was disinfected using a chlorhexidine solution (Klorhexidin, Fresenius Kabi). A one cm skin incision was made using an operation scissor. The skin was separated to expose the temporal muscle where a droplet of saline (9 mg/ml Natriumklorid, Fresenius Kabi) was applied. To avoid bleeding, a high-frequency generator (VIO 50C, Erbe), was set to 12 W and bipolar mode before the diathermic forceps was used to detach the temporal muscle from the skull at its apical and distal parts to create a muscle flap. Underneath the MCA was located through the transparent skull (figure 1). Using a drill (Dremel), the skull was thinned directly above the MCA, and the last thin layer of bone was gently removed using ultrafine forceps under a microscope. The high-frequency generator was set to 7 W and the diathermic forceps was used to coagulate the MCA both proximally and distally to the first bifurcation downstream of the lenticulostriate arteries (M1 to M2). Both sides of the diathermic forceps was gently placed close to both sides of the artery (without directly touching it) an power was applied to coagulate the artery. After a 30 second wait, the artery was gently touched with blunted forceps to check for reperfusion. At any sign of reperfusion, the electrocoagulation was repeated.

Figure 1 - The MCA was permanently coagulated both proximal and distal to the bifurcation.

After the electrocoagulation, the temporal muscle was placed back to its position and the incision wound was sutured. The mice were placed in a nurturing box with the temperature set to 32 °C to recover from the anaesthesia before they were moved back to their home cage. Buprenorphine 0.1 mg/kg i.p. was administered 24 hours after the operation and daily thereafter for four days to provide postoperative analgesia.

Sham operation

Sham operations were performed on three mice as procedure control. The operations were performed identically including thinning of the skull. However, removal of the last layer of bone and electrocoagulation was not performed.

3.3 Preparation of samples

3.3.1 Perfusion fixation - *In Vivo* fixation

Introduction

In order to extract the brains while preserving the integrity of the tissue, perfusion fixation was performed. During perfusion fixation, the circulatory system of the mouse is utilised to distribute the fixation medium to all tissues of its body (114). The goal is to rapidly replace the animal's entire blood volume with fixative to minimise hypoxic damage to the CNS tissue (115). It is key to maintain the systolic blood pressure, as even brief reductions will lead to some degree of vascular collapse, which in turn may inhibit the distribution of the fixative to certain tissues. Too high pressure may cause brain swelling and oedema. The rate at which the fixative is pumped through the circulatory system should therefore mimic the

animal's cardiac output. The procedure is terminal, which requires the animal to be heavily anaesthetized prior to the operation.

The fixation solution used was 4% paraformaldehyde (PFA) in 0.1M sodium phosphate (NaPi) buffer with pH 7.4. PFA is a formaldehyde (FA) polymer that, when treated with heat and sodium hydroxide, is hydrolysed to single carbon FA monomers (116). FA is an electrophilic, highly reactive fixative (114, 117). When introduced to a tissue, FA initially reacts with primary/terminal amines (lysine), purines and thiols (cysteine) and forms a methylol intermediate (114, 117). Over the next 24-48 hours, these intermediates can condensate and yield an imine (Schiff base) that subsequently reacts with a new nucleophilic group from the same or another cellular compound. This process is called cross-linking and creates covalent methylene bridges between reactive groups on cellular compounds.

Procedure

The mice were anaesthetized with an i.p. injection of ZRF-mix (zolazepam 3.3 mg/ml, tiletamin 3.3 mg/ml, xylazine 0.5 mg/ml, and fentanyl 2,6 µg/ml), 0.1 ml/g bodyweight, provided by the facilities veterinary. After a five-minute wait, a toe-pinch-test was performed (as described above) to ensure that the mice had reached a surgical plane of anaesthesia. If no reflex was observed, the mice were mounted in a supine position with their limbs spread on a shallow styrofoam plate using cannulas. The plate was placed in a fume hood together with the peristaltic pump (Watson-Marlow, 323) and the operation equipment needed to perform the perfusion.

The procedure began with a traverse skin incision below the diaphragm and a medial skin incision over the abdomen of the mice, which exposed their abdominal organs. Next, the sternum was cleaved medially, and their rib cage was folded away to expose the thoraxic organs. From this step on, the rest of the procedure was performed as quickly as possible, to avoid hypoxic conditions, since the lungs collapse when the diaphragm is perforated. The cannula, attached to the peristaltic pump, was inserted in the left ventricle of the heart simultaneously as the right auricle was perforated. The fixation fluid pump rate was kept at 5 ml/min for 8 minutes while visual indicators of the progress were monitored (stiffing of the body, extension of the tale and bleaching of the liver). Finally, the mice were decapitated, and their skulls were gently opened medially from the foramen magnum and along the sagittal suture using a pair of scissors. Care was taken not to touch the brain with the scissors. The

bone was folded away, and the brain was removed and stored in a 4% PFA solution at refrigerated temperature over night. The brain was then transferred to a 0.4% PFA solution and kept at refrigerated temperature for storage until further processing.

3.3.2 Cryosectioning of fixed mouse brains

Cryoprotection

Before sectioning, the brains were transferred to 30% sucrose solution with 0.1 M sodium phosphate (NaPi) in individual tubes at refrigerated temperature. The brains were allowed to saturate overnight, to provide cryoprotection for the fixed tissue.

Sectioning

In order to section the fixed mouse brains for further examination, sliding microtomes were used (HM 450, Thermo Fisher Scientific). These microtomes operate with a static tissue plate and a sliding steel knife. They were equipped with tissue freezing units, which allowed for rapid freezing and cryosectioning of the fixed brains.

In preparation, tissue culture plates with 12 wells (3 x 4 wells marked A1 to C4) were prepared (VWR® Tissue culture plates, 12 wells, sterile). Using a multipipette (Eppendorf® Multipitette® Plus), each well was filled with 5 ml 0.1 M NaPi buffer with 0.05 % sodium azide to ensure that the sections were kept conserved in physiological pH (7.4). Four plates were prepared for each brain and marked one to four.

The brains were individually transferred to a petri dish. Using a razor blade, a coronal cut was made 5-6 mm caudal of the inferior colliculus, leaving a flat posterior surface. An ice stage (measuring approximately 2 cm x 2 cm x 0.5 cm) was made by dripping 30% sucrose solution on to the microtome freezing plate with the temperature set to -40 °C using a disposable pipette. The steel knife was use to trim a flat surface on which the brains could be mounted. The brains were placed with the flat posterior surface facing down on the stage, allowed to freeze entirely and stabilised in ice by gradually dripping 30% sucrose solution on and around the brain. Thereafter the freezing plate temperature was adjusted to -20 °C and the brains were coronally serial sectioned into 20 μm sections that melted on the room-tempered knife. Using a small paintbrush with pine marten hair (Panduro Hobby 0.3 mm and 1.0), the sections were systematically transferred to separate wells in an increasing order from

well A1 on plate one to well C4 on plate four. This system was repeated, as shown in figure 2, until the entire brain had been sectioned. This allowed later extraction in a systematic manner. The tissue culture plates were then covered in parafilm and stored refrigerated until mounting and further analysis.
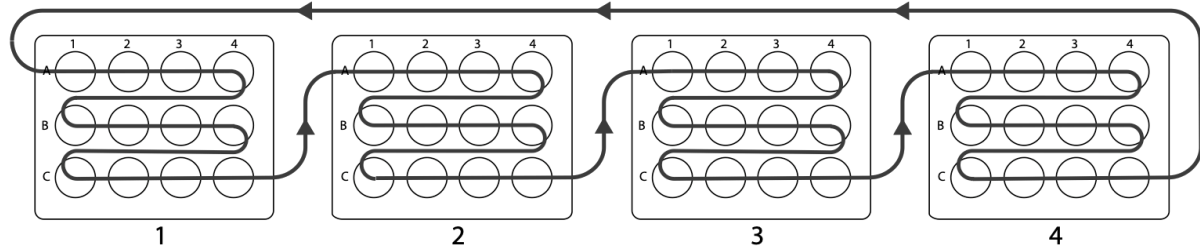
Figure 2 The sections were placed in wells in an increasing order from well A1 on plate one to well C4 on plate four to keep the sections in a chronologic order for later extraction.

3.4 Measurement of lesion volume

3.4.1 Mounting of tissue sections

The 20 μm thick sections of brain tissue were mounted to 25 x 75 x 1.0 mm glass slides (Superfrost Plus, Thermo Fisher Scientific) under a microscope (M60 stereo microscope, Leica). These slides have a permanent positive charge to electrostatically attract the tissue sections. Every 8th section was mounted unless they were damaged or other circumstances made it necessary to use the neighbouring section. To achieve an even and unwrinkled result, a droplet of water (ca. 120 μl) was placed on the glass slides. Each free-floating section was removed from their well using a small paintbrush with animal hair (Panduro Hobby 0.3 mm and 1.0 mm pine marten hair) and placed in the droplet. While slowly removing the water, the paintbrush was used to adjust and straighten the sections under the microscope. Six sections were mounted per glass slide before they were left to dry in room temperature for 1-2 hours to ensure that the sections were properly attached to the glass slides for the subsequent the staining procedure.

3.4.2 Nissl staining of mounted tissue sections

The glass-mounted sections were stained using cresyl violet dye. Cresyl violet is a cationic, hydrophilic oxazine dye that binds electrostatically to negatively charged cellular structures like RNA and DNA (118). It therefore labels the rough endoplasmic reticulum (nissl body), nucleus and other accumulations of nucleic acid by staining them bluish-purple. Cresyl violet staining is commonly used for histological examination of neuronal tissue.

After some optimisation, a customized regressive staining protocol was developed. The detailed procedure is given in Table 1. In short, the tissue was stained before the surplus dye was removed by acidic differentiation. The procedure involved four main steps:

   i.   Rehydration: The glass-mounted tissue sections were treated with a series of ethanol in decreasing concentration followed by distilled water. Due to the hydrophilic nature of cresyl violet, rehydration is necessary to improve the distribution of the dye into the tissue.

  ii.   Staining: The tissue sections were treated with 0.1% cresyl violet acetate (3.1 mM) in distilled water for eight minutes at 60 °C using a water bath. The solution was heated to 60 °C and filtered using a paper filter (VWR folded qualitative filter paper, particle retention 10-20 μm) to avoid any undissolved cresyl violet particles before the staining procedure.

 iii.   Washing and differentiation: Following the cresyl violet treatment, the sections were washed to remove the excess dye, first in distilled water followed by 95 % ethanol. Cresyl violet will be ionised and readily removed from the tissue in an acidic environment. Therefore, the sections were treated with 1% glacial acetic acid in 95% ethanol for approximately three seconds and immediately rinsed in 95% ethanol to stop the process. This process is commonly referred to as differentiation and is performed to remove any excess dye, leaving the structures with the highest affinity to cresyl violet highlighted. The sections were visually inspected to ensure that the staining was adequate for further analysis. Overstained sections were differentiated for a few additional seconds while understained sections were restained by repeating the protocol from the rehydration step.

  iv.   Dehydration and mounting: after dehydration in 95% alcohol, the stained sections were treated with a xylene substitute (Neo-Clear, Merck) to remove the remaining water before a coverslip was mounted with a few droplets of mounting medium (Neo-Mount, Merck).

Table 1 Nissl staining protocol

No.	Agent	Time
1	95% ethanol	15 minutes
2	70% ethanol	1 minute
3	50% ethanol	1 minute
4	Distilled water	2 minutes
5	Distilled water	1 minute
6	Cresyl violet - 1 g/L at 60 °C	8 minutes
7	Distilled water	1 minute
8	Distilled water	1 minute
9	95% ethanol	1 minute
10	1% glacial acetic acid in 95% ethanol	3 seconds
11	95% ethanol	5 seconds
12	95% ethanol	1 minute
13	Neo-Clear	1 minute

3.4.3 Light microscopy

Surface images of the nissl-stained coronal sections were attained at 20x magification using a automated slide scanner system (Axio Scan Z1, Carl Zeiss Microscopy, Germany; SteREO Lumar V12, Carl Zeiss Microscopy, Germany).

3.4.4 Volumetric infarct analysis after permanent occlusion of distal middle cerebral artery

The digital surface images of the coronal nissl stained sections were analysed using FIJI (Image J, version: 2.0.0-rc-69/1.52i). The image files included a pixel per distance ratio. This allowed for the measurement of regions of interest by outlining them and converting the pixels within the outline to a metric (square millimetres - mm^2). The outlining was saved as "region of interest" (ROI) files. The lesion area in each section was calculated by subtracting the cortical area of the ipsilateral hemisphere (excluding the stroke lesion) (ICA) from cortical area of the contralateral hemisphere (CCA) in each section (known as the Swanson Method (119)) (Figure 3).
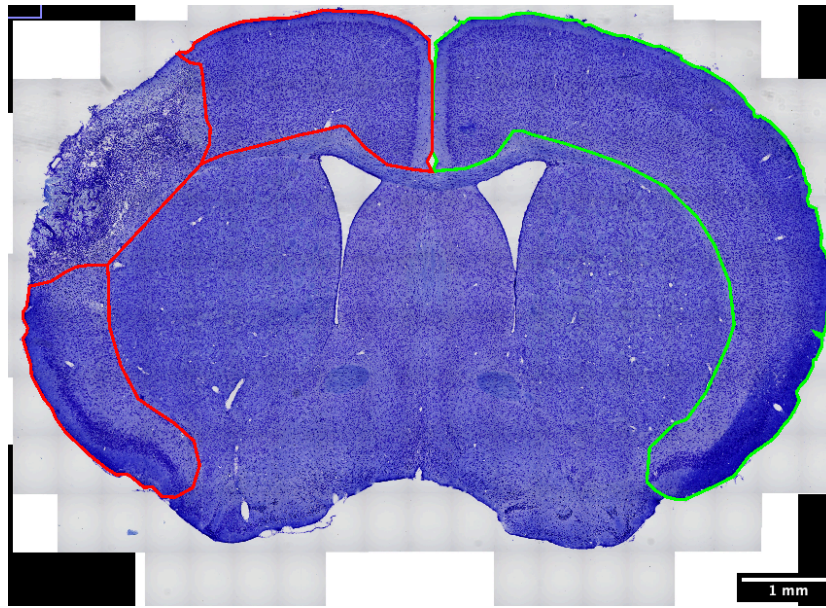
Figure 3 Measurement of difference in cortical area illustrated in coronal section at 0.5 mm rosrtal of bregma. Ipsilateral cortical area (ICA) (red) was subtracted from the contralateral cortical area (CCA) (green)

The lesion area was calculated for every 8th 20 μm thick section between 1.5 mm rostral and 2.5 mm dorsal of bregma (n), 4 mm in total. The lesion volume was calculated by summarising the difference in cortical area multiplied by 4 mm / n for each section.

$$LVa = \sum_{k=1}^{n} ((CCA - ICA) \times \frac{4\ mm}{n})_k$$

The measurements were performed by blinded technicians. Comparing ROI files from a sample of sections with measurements made by a supervising technician ensured reproducibility.

3.5   Immunohistochemistry

In order to compare the expression of local immune cells in the perilesional tissues, both peroxidase and fluorescent immunohistochemical (IHC) procedures were performed on brains extracted one week after permanent distal MCAO. The principle of IHC is to use antibodies (Abs) that bind to specific target antigens and subsequently visualise them, using a secondary antibody coupled to a ether a flourophore (fluorescent IHC) or an enzyme that catalyses a chemical reaction yielding a colored precipitate (colorimetric IHC) (120).

The goal of the IHC procedures was for the Abs to bind selectively to the antigen. Binding to various unintended structures in the tissue would result in nonspecific background staining (121). To minimise nonspecific binding, the tissue was treated with a blocking solution consisting of newborn calf serum (NCS) and bovine serum albumin (BSA) in 0.5% triton in PBS. The serum proteins bind to the nonspecific epitopes, making them inaccessible for the primary Abs. In tissue fixed with formaldehyde, cross-linking may conceal the epitopes of interest (122). It was therefore necessary to perform an antigen retrieval by treating the fixated tissue in an alkaline buffer at a high temperature to break the formaldehyde-related crosslinks and unfold inner epitopes.

3.5.1 Buffers and solutions

Phosphate-buffered saline (PBS) pH 7.4

9.8 mM di-Sodium hydrogen phosphate dihydrate, 137 mM sodium chloride, 2.7 mM potassium chloride, 2 mM potassium dihydrogen phosphate, in milli-Q water

Blocking solution

3% newborn calf serum (NCS), 1% bovine serum albumin, 0.5% triton, in PBS

Citrate buffer

114 mM sodium citrate, in milli-Q water.

3.5.2 Peroxidase immunohistochemistry

Introduction

A qualitative peroxidase ICH procedure was performed in order to establish a general opinion of which anatomical location would be best suited for the subsequent quantitation of microglia. Therefore the goal of this procedure was to stain the Iba1-positive cells present in the selected sections in order to look for morphological signs of microglia activation as an indication for subsequent quantification microglia density.

The staining method used is commonly known as the 3,3-diaminobezidine (DAB) staining method (120). The method is based on an avidin-biotin complex (ABC) reaction. In short terms, the procedure included four mains steps:

i. The tissue was incubated with a primary Ab, selective for the tissue antigen of interest.

ii. The tissue was incubated with a biotinylated secondary Ab, selective for the Fc region of the primary Ab.

iii. The tissue was incubated with a streptavidin-biotin-enzyme complex. The avidin/streptavidin will selectively bind to the biotin on the secondary Ab.

iv. The tissue was treated with a substrate for the enzyme, bound to the antigen of interest.

The primary AB has two binding sites for the secondary Ab, thereby amplifying the signal from one, to two potential signal molecules per epitope. Sreptavidin has four binding sites for biotin, and will bind to the biotin on the secondary Ab as well as biotin bound to other streptavidin-biotin-enzyme complexes, thereby amplifying the signal. In the final step, horseradish peroxidase (HRP) binds to the streptavidin-biotin-complexes. DAB is oxidised to a dark brown precipitate by hydrogen peroxide in a reaction catalysed by HRP. The formation of DAB precipitate visualises the locations where the antigen is expressed. It is therefore important to eliminate any peroxidase enzymes endogenously present in the tissue before the procedure to avoid unspecific DAB oxidation. Iba1 was chosen as the target antigen for microglia labeling, as microglia is morphologically easy to distinguish from other Iba1-positive cells.

Procedure

Two 6 x 4 well plates (Nunclon 24-well cell culture plates, Thermo Fisher Scientific) were prepared and each well was filled with 1 ml phosphate-buffered saline (PBS), pH 7.4. One section from each brain was selected and placed in separate wells, 37 sections in total. One surplus section was included as a primary antigen negative control. The sections were selected from the area between 1.3 mm rostral and 0.1 mm dorsal of bregma. The procedure was executed as described in Table 2 and Table 3. The negative control was incubated in blocking solution without primary Ab:

Table 2 Peroxidase staining protocol; day one.

No.	Procedure	Time
1	Wash with PBS	2 x 10 minutes
2	Antigen retrieval - citrate buffer, pH 8.6; 80 °C	30 minutes
3	Wash with PBS	3 x 10 minutes
4	Elimination of endogenous peroxidases - 2% H_2O_2 in PBS	
5	Wash with PBS	3 x 10 minutes
6	Blocking in blocking solution	60 minutes
7	Incubation with primary Ab in blocking solution - Iba1 WAKO from rabbit; 1:2000	Over night

Table 3 Peroxidase staining protocol; day two.

No.	Procedure	Time
8	Wash with PBS	6 x 10 minutes
9	Incubation with biotinylated secondary Ab in blocking solution. Anti-Rabbit IgG, Horseradish Peroxidase linked whole antibody from donkey; 1:100	60 minutes
10	Wash with PBS	3 x 10 minutes
11	Incubation with Biotin-streptavidin-HRP complex; 1:100 in blocking solution	60 minutes
12	Wash with PBS	3 x 10 minutes
13	DAB in PBS (5 mg tablet per 20 ml)	6 min
14	PBS with DAB (1 tablet per 20 ml) and 0.01% H_2O_2	Observed under a microscope until desired result
15	Wash with PBS	3 x 10 minutes

After the staining procedure, the sections were mounted to 25 x 75 x 1.0 mm glass slides (Superfrost Plus™ from Thermo Scientific™), dried for 5 minutes before a cover slip was mounted using melted glycerine-gelatine.

3.5.3 Light microscopy

Surface images of the peroxidase-stained coronal sections were attained at 40x magification using a automated slide scanner system (Axio Scan Z1, Carl Zeiss Microscopy, Munich, Germany; SteREO Lumar.V12, Zeiss, Germany).

3.5.4 Fluorescent immunohistochemistry

Introduction

In order to quantify the density of microglial in and around the penumbra, fluorescent IHC was performed. Considering the fact that microglia migrate and rapidly proliferate in response to inflammation and tissue damage, microglial density was chosen as a marker for degree of inflammation (50, 51). For this purpose, Iba1 was once again chosen as the target antigen (se above). Based on the DAB-labeling, suitable and easily reproducible areas of interest for the fluorescent IHC was determined. Coronal sections from 1.1 mm rostral of bregma were used.

The procedure included two main steps;
  i)   Primary Ab labeling
  ii)   Secondary Ab and 4,6-diamidino-2-phenylindole (DAPI) labeling. The principal of primary and secondary Ab labeling is similar that in colorimetric IHC, except that secondary Abs are conjugated with a fluorophore, designed to emit fluorescent light when irradiated with light at a specific wavelength.

Procedure

Two 6 x 4 well trays (Thermo Fisher Scientific, Nunclon 24-well cell culture plates) were prepared and filled with 1 ml (PBS), pH 7.4. One section from each brain was selected and placed in separate wells. One surplus section was included as a primary antigen negative control. The procedure was executed as described in Table 4 and Table 5. The negative control was included in all steps, except the primary Ab was omitted in step 4:

No.	Procedure	Time
1	Antigen retrieval - citrate buffer, pH 8.6; 80 °C	30 minutes
2	Wash with PBS	3 x 10 minutes
3	Blocking with blocking solution	120 minutes
4	Incubation with primary Abs blocking solution. Iba1 WAKO from rabbit; 1:500	Over night

Table 5 Fluorescent ICH labeling protocol; day two

No.	Procedure	Time
1	Wash with PBS	6 x 10 minutes
2	Incubation with secondary Abs in blocking solution. Donkey-anti-rabbit Alexa Fluor 488;	120 minutes
3	Wash with PBS	3 x 10 minutes
4	Incubation with DAPI; 1:5000 in PBS	15 minutes
5	Wash with PBS	3 x 10 minutes

The stained sections were mounted on separate 25 x 75 x 1.0 mm glass slides (Superfrost Plus, Thermo Scientific), dried for 5 minutes before a cover slip was mounted using a anti photobleaching mountant (ProLong Gold, Thermo Fisher Scientific). Mounted tissue sections where stored shielded from light at refrigerated temperature.

3.5.5 Confocal microscopy

Introduction

Images were taken at four areas in each section: lateral and medial (cortex and striatum, respectively) of the corpus callosum in both hemispheres (Figure 4).
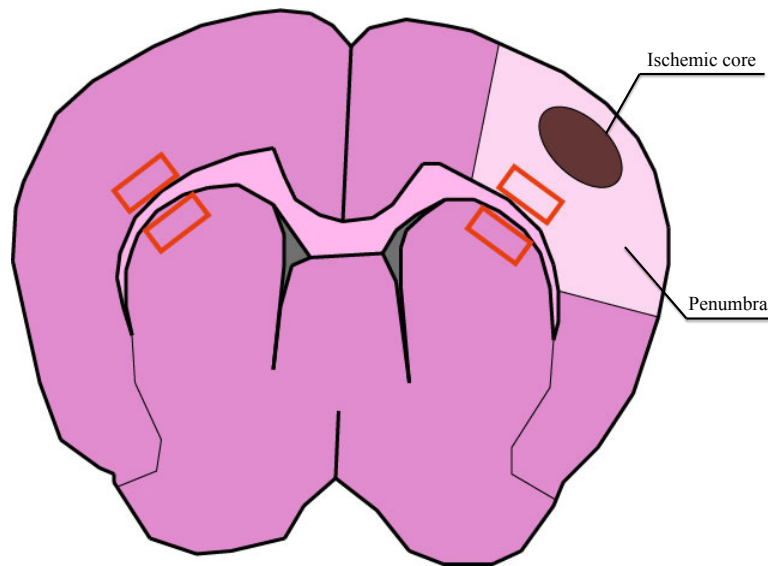
Figure 4 Simplistic illustration of areas scanned in coronal sections 1.1 mm rostral of bregma

Procedure

The mounted immunolabeled tissue sections were analysed with a confocal microscope (Zeiss LSM880 - Fast Airy Scan). Initially, he appropriate lasers for the immunolabeling were activated: Alexa 405 for DAPI and Alexa 488 for Iba1. Suitable laser intensity and gain was adjusted and saved as a pre-setting. All scans were performed with the same pre-setting for consistent intensity in all images. A 1056 μm x 457 μm x 20 μm three-dimensional scan was performed at each pre-determined area of interest at 20x magnification. Before each scan, the Z-stack position was adjusted to correct for any vertical variation with in the section.

3.5.6 Analysis of confocal microscopy scans - measurement of microglia density

The three-dimensional scans attained by confocal microscopy was analysed using FIJI (Image J, version: 2.0.0-rc-69/1.52i). All visible microglia present in the images were marked and counted manually. The Iba1-labeling visualised the cell body, and the DAPI-labeled nucleuses was consulted to ensure that all microglia was adequately counted. The number of microglia per 1056 μm x 457 μm x 20 μm scan was counted and converted to microglia per mm^3.

3.6 Statistics

All statistics in the present study was performed in IBM SPSS statistics 25, Microsoft excel or GraphPad Prism 8. One-way analysis of variance (ANOVA) and Turkey´s range test (post-hoc) was performed as equal variance was assumed. When appropriate, paired student t-tests and linear regression was performed. Differences with p-values < 0.05 were considered significant. All data are presented as average ± standard deviation (SD).

4 Results

Following the occlusion operation, six male wt, five female wt, one male HCAR1 KO, and÷one female KO mice died prior to day seven (when brains from the one-week-group were to be extracted). The female wt mice were all housed in the same cage, and it can not be excluded that their premature death might have been the result of a malfunctioning cage or other causes that are not related to the treatment. If these mice are included, we have a higher death rate among wt mice than among KO mice (4.7%, p=0.006; chi square test; Microsoft Excel; p = 0.096 if the five wt females are excluded).

4.1   Lesion volume

Lesion volumes from brains extracted one or three weeks after permanent electrocoagulation of the distal MCA was measured. In the interest of determining whether the difference in average lesion volume was due to lactate-HCAR1 interaction, lesion volumes from HCAR1 KO lac, HCAR1 KO sal, wt lac, and wt sal mice were compared within the one and three week groups.

Lesion volumes < 3 mm^3 and > 20 mm^3 was considered outliers and excluded. In the brains where lesion volumes < 3 mm^3 was observed, there were few or no signs of infarction indicating that the occlusion procedure had been unsuccessful (one week: one wt sal, three wt lac, two KO sal, and three KO lac; three weeks: 1 KO lac, and 2 wt lac). In mice that were excluded due to lesion volume being > 20 mm^3, there were signs of a secondary cerebral haemorrhaging and the lesion extended over the corpus callosum and in to the ipsilateral striatum (one week: one wt lac and one KO lac).

4.1.1 Lesion volumes at one week after stroke

In the sections from the one-week-group the lesions were plainly visible and infarcted and healthy tissue were easy to distinguish (figure 5). In the most affected brains, the infarction bordered corpus callosum for large extents of the barrel cortex. The infarcted tissue was fragile and demanded great care during the section mounting. In occasional sections the infarcted tissue was missing.
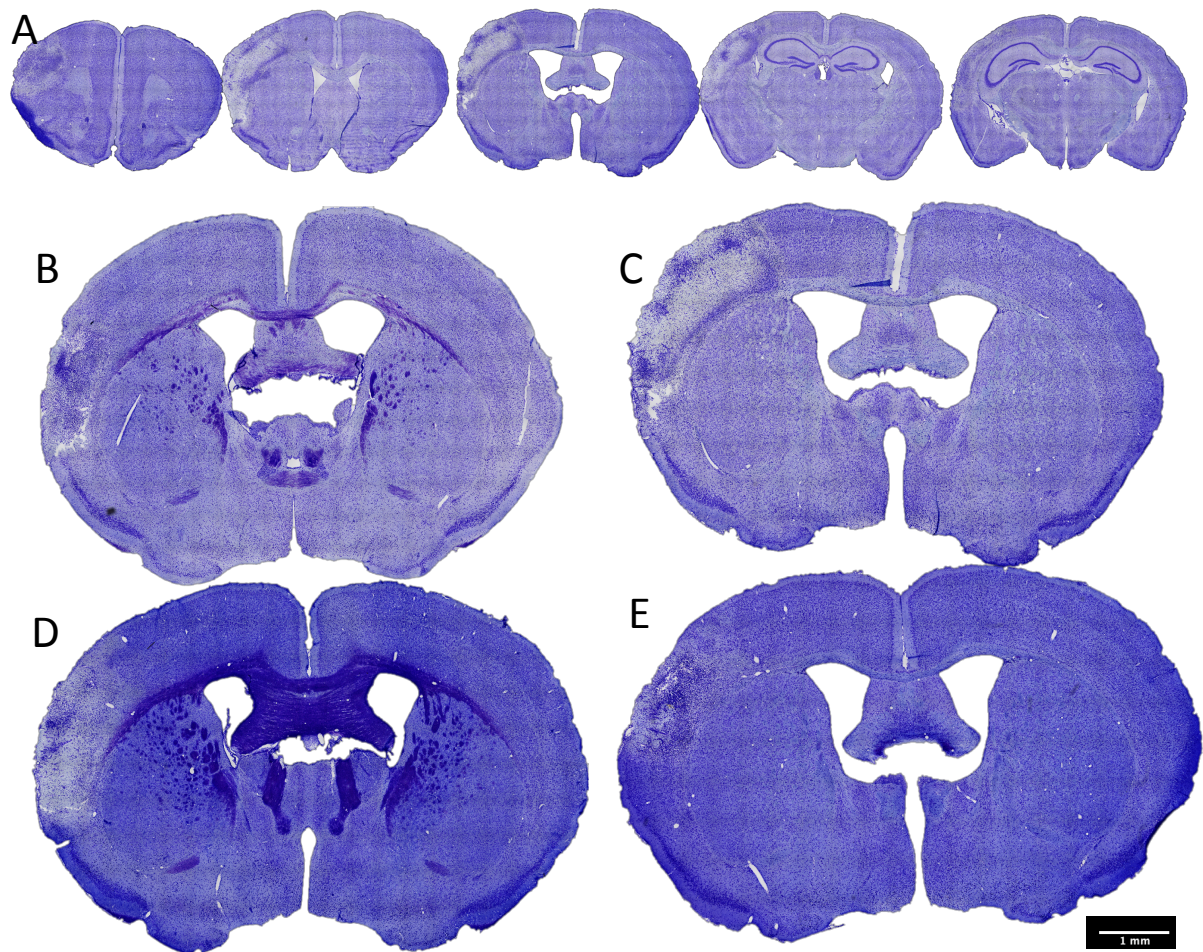
Figure 5 All sections in this figure stems from brains extracted one week after permanent electrocoagulation of the distal MCA. **A)** Sample of coronal sections between 1.5 mm rostral and 2.5 mm dorsal of bregma. Coronal section at 0.4 mm dorsal bregma from the brain of **B)** wild-type (wt) mouse treated with saline (sal), **C)** wt mouse treated with lactate (lac), **D)** HCAR1 knock-out (KO) mouse treated with sal, **E)** KO mouse treated with lac. Scale bar: 1 mm.

There were no significant differences between any groups in the average lesion volumes one week after the permanent distal MCAO procedure (figure 6)
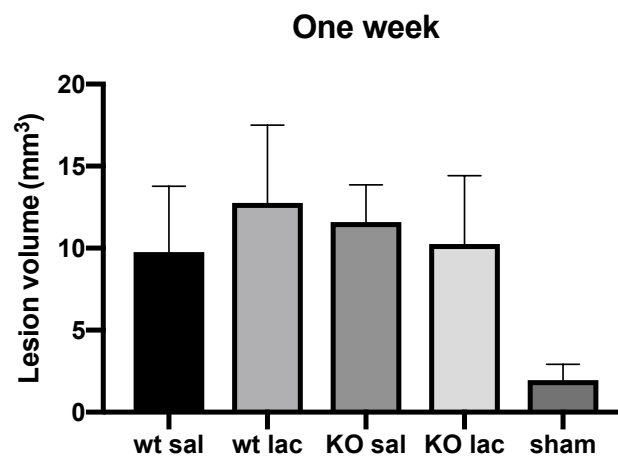
Figure 6 Average lesion volume (LV) measured in brains from wild-type (wt) mice treated with saline (sal) (9.76 ± 4.01, n = 4) and lactate (lac) (12.77 ± 4.74 mm^3, n = 3), and HCAR1 knock-out (KO) mice treated with sal (11.60 ± 2.27 mm^3, n = 6) and lac (10.26 ± 4.16 mm^3, n = 7) one week after permanent distal middle cerebral artery occlusion (MCAO) (Sham: 1.95 ± 0.97 mm^3, n = 3). There was no significant difference between the groups (one-way ANOVA, SPSS).

4.1.2 Lesion volumes at three weeks after stroke

In the brain sections from mice three weeks after stroke induction, the infarction resembled scarred tissue and was mainly visible as a general thinning of the ipsilateral cortex (figure 7).

Figure 7 All sections in this figure stems from brains extracted three weeks after permanent electrocoagulation of the distal MCA. **A)** Sample of coronal sections between 1.5 mm rostral and 2.5 mm dorsal of bregma. Coronal section at 0.4 mm dorsal bregma from the brain of **B)** wild-type (wt) mouse treated with saline (sal), **C)** wt mouse treated with lactate (lac), **D)** HCAR1 knock-out (KO) mouse treated with sal, **E)** KO mouse treated with lac. Scale bar: 1 mm.
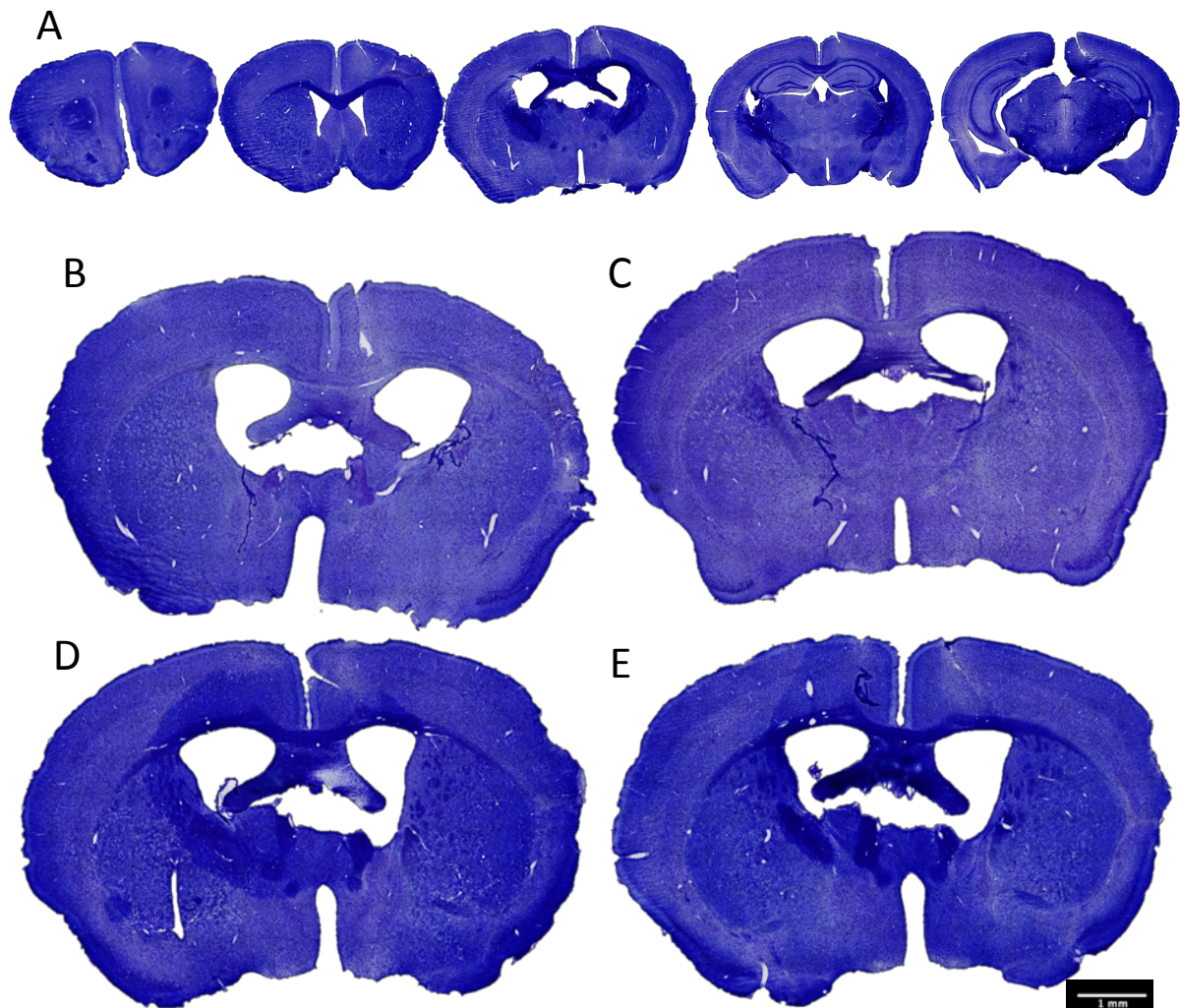
After three weeks, an HCAR1-dependent reduction in the lesion volume in response to lactate treatment was detected: the average lesion volume in in the wt lac group was significantly smaller than in the wt sal group (p = 0.003; one-way ANOVA, Tukey´s post hoc test). This effect of lactate was not found in the KO group, as the lesion volume measured in KO lac was not different form the lesion volume in KO sal (p = 0.590; one-way ANOVA, Tukey´s post hoc test). Interestingly, both groups of KO mice tended to show smaller lesion volumes than the wt sal group, but this was only significant for the KO lac (p = 0.005; one-way ANOVA, Tukey´s post hoc test, SPSS). The results from the measurements are displayed in (figure 8)
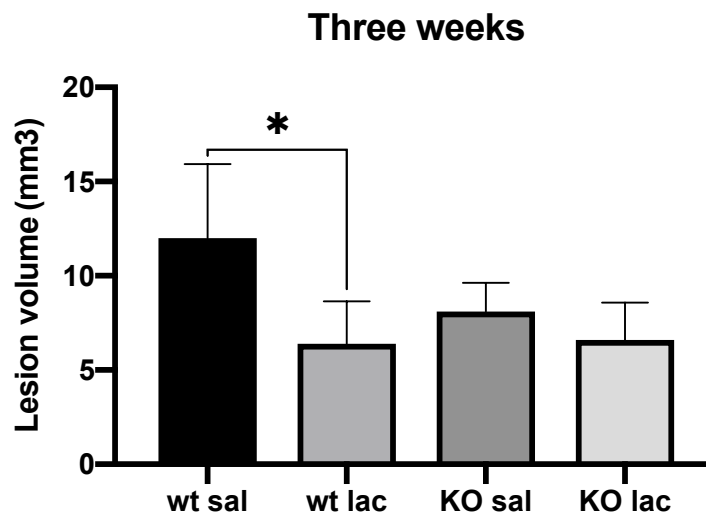
Three weeks

Figure 8 Average lesion volume measured in brains from wt mice treated with sal (12.00 ± 3.92 mm^3, n = 4) and lac (6.40 ± 2.25 mm^3, n = 8), and HCAR1 KO mice treated with sal (8.11 ± 1.52 mm^3, n = 7) and lac (7.04 ± 1.92 mm^3, n = 8) three weeks after permanent distal MCAO. * p < 0.05 (one-way ANOVA, Tukey post hoc test, SPSS).

Average sizes in all treatment groups except for wt sal was significantly smaller three weeks after induction of stroke compared to one week (wt lac: p = 0.0117, KO sal: p = 0.0003, KO lac: p = 0.0121, paired students t-test, Microsoft excel). The average lesion size in the wt sal group was not significantly different at one and three weeks after stroke (p = 0.4542, paired students t-test, Microsoft excel)

4.2 Peroxidase immunohistochemistry

Microglia proliferate and migrate to areas of injury through detection of chemoattractant gradients of inflammation. Therefore, microglial density was quantified in brains extracted one week after permanent occlusion of the distal MCA as an indication for the degree of inflammation in the analysed areas. To determine whether an HCAR1-dependent alteration in neuroinflammation may explain the effect of lactate treatment in wt animals after three weeks, that is not detectable after one week, the density of Iba1 positive cells was investigated. Iba1 does not separate between intrinsic immune cells of the brain (microglia) and extrinsic, blood-born immune cells (machrophages ect). For simplicity, all Iba1 positive cells are occasionally referred to as microglia in the following text.

First, a pilot study a using peroxidase IHC procedure was performed in order to determine which areas would be optimal for a subsequent detailed microglia density measurement by fluorescent IHC. During the mounting of nissl-stained sections, the impression was that the

lesion in the brains extracted one week after permanent distal MCAO was consistently well affirmed in the region of 1.3 mm rostral to 0.1 mm dorsal of bregma. Therefore, the peroxidase IHC was performed on sections within this interval. The aim was to determine areas where the tissue consistently could be considered part of the penumbra, i.e. not necrotic nor unaffected, assessed by microglia morphology. The areas on the cortical side of the corpus callosum, consistently showed no necrosis, but still the tissue was clearly affected by the stroke. In this area, we saw an increased density of Iba1-positive cells, with morphology than indicated microglia activation. The morphology of the Iba1-positive cells in this area was different from the apparently resting microglia found in the same area on the contralateral side. Similarly, in the underlying ipsilateral striatum, there was also an apparent increase in Iba1 intensity compared to the contralesional side. Figure 9 represents the general tendency that was observed. The areas adjacent to the corpus callosum, were determined the best suited areas (see figure 4).
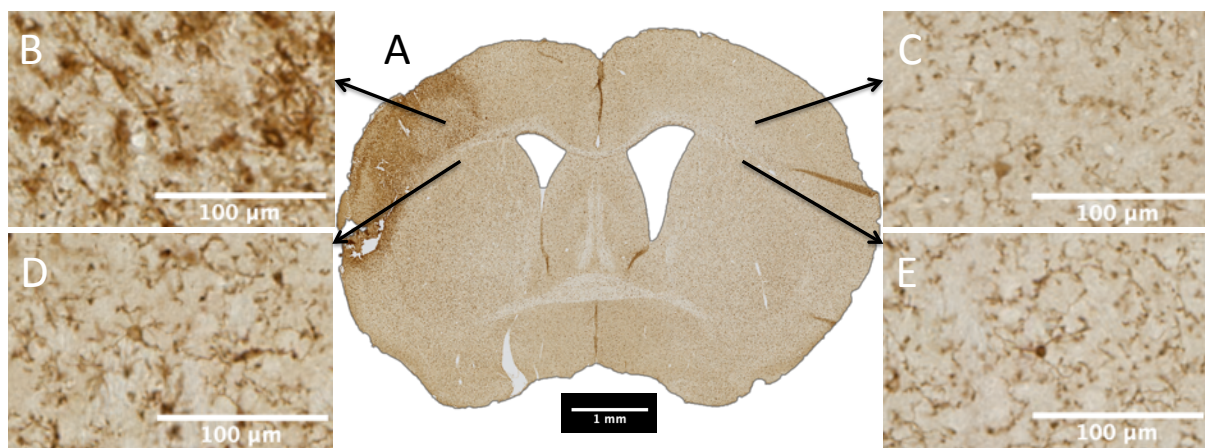
Figure 9 General representation of microglia morphology in the areas determined as suitable for subsequent microglia density measurement. **A)** Macro image of an Iba1-peroxidase stained section. Scale bar: 1 mm. Micro image of Iba1-positive cells in **B)** ipsilateral cortex, **C)** contralateral cortex, **D)** ipsilateral striatum, **E)** contralateral striatum. Scale bars are 100 μm in B-E.

4.3   Density of Iba1-positive cells

The density of Iba1-positive cells (number of cells/mm3) in the four areas of interest was measured manually in the three-dimensional z-stacks attained by fluorescent IHC and confocal microscopy of coronal sections 1.1 mm rostral of bregma (as described above). Two sections were lost during the IHC procedure: one HCAR1 KO lac, and one wt sal. Mice that were considered outliers after measurement of lesion volume were not included. The group sizes were as follows: wt sal, n = 3; wt lac, n = 3, KO sal, n = 6; KO lac, n = 6; sham, n = 3.

4.3.1 Microglia density

The sections stained for Iba1 yielded strong and easily recognisable microglia-like labeling when assessed in a confocal microscope (figure 10). The microglia present in the 1056 μm x 457 μm x 20 μm region of interest was quantified and the density of microglia (number of cells per mm^3) was calculated.
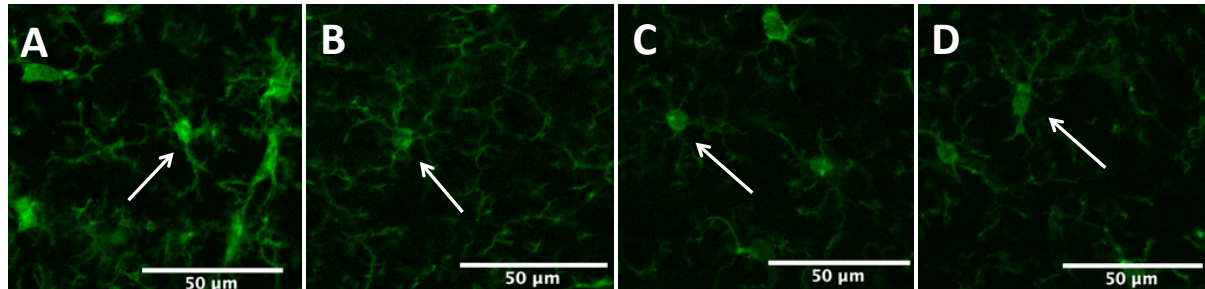
Figure 10 All pictures are from a wild-type saline treated mouse. The scale bar represents 50 μm. **A**: Iba1-positive cell in the ipsilateral cortex. **B**: Iba1-positive cell in the ipsilateral striatum. **C**: Iba1-positive cell in the contralateral striatum. **D**: Iba1-positive cell in the contralateral striatum.

Regardless of treatment, there was a significant linear correlation between larger stroke volumes and higher density of Iba1-positive cells, with sham operated animals showing the lowest density (figure 11). A similar trend was observed in the ipsilateral striatum, although the sham-operated animals were less different from the animals with stroke.
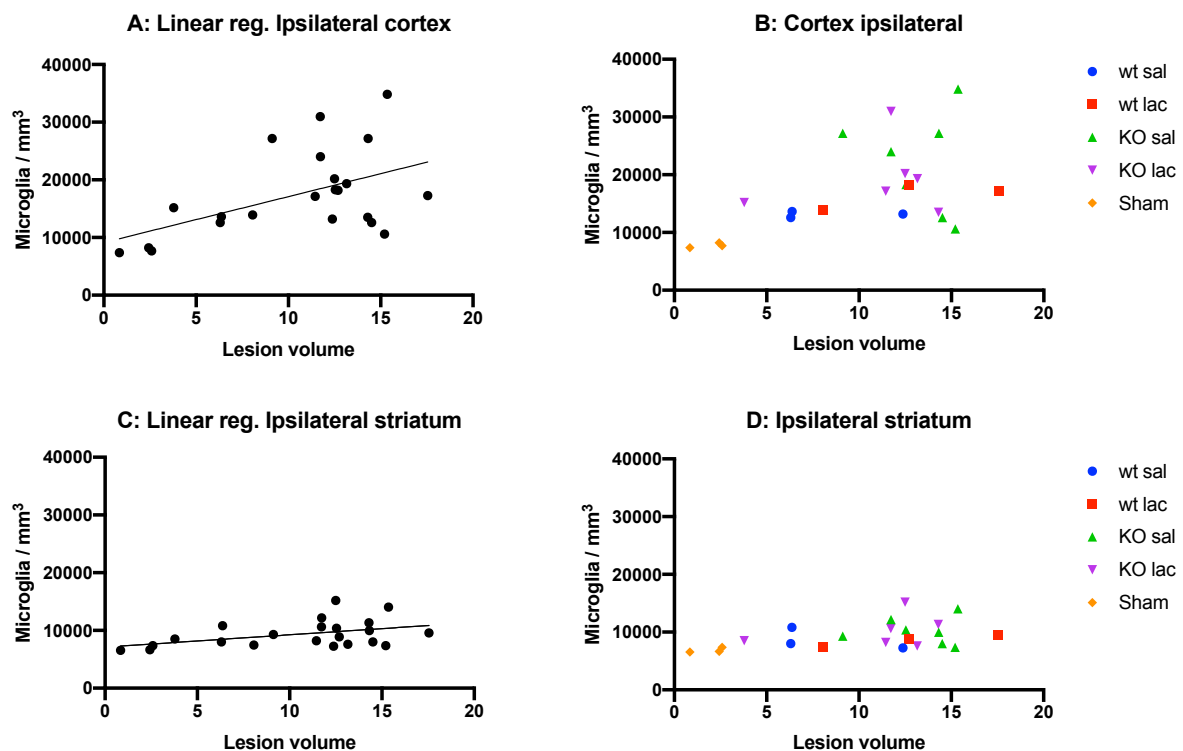
Figure 11 A: Linear regression of the relationship between lesion volume and microglia density in the ipsilateral cortex (p = 0.016, R^2 = 0.2579, linear regression, GraphPad). **B:** Scatter plot of the relationship between microglia density and lesion volume in ipsilateral cortex, separated by genotype and treatment groups. **C:** Linear regression of the relationship between lesion volume and microglia density in the ipsilateral striatum (p = 0.041, R^2 = 0.1934, linear regression, GraphPad). **D:** Scatter plot of the relationship between microglia density and lesion volume in ipsilateral cortex, separated by genotype and treatment groups.

Although the average microglia density generally was higher in the KO mice, there were no significant differences between any groups.
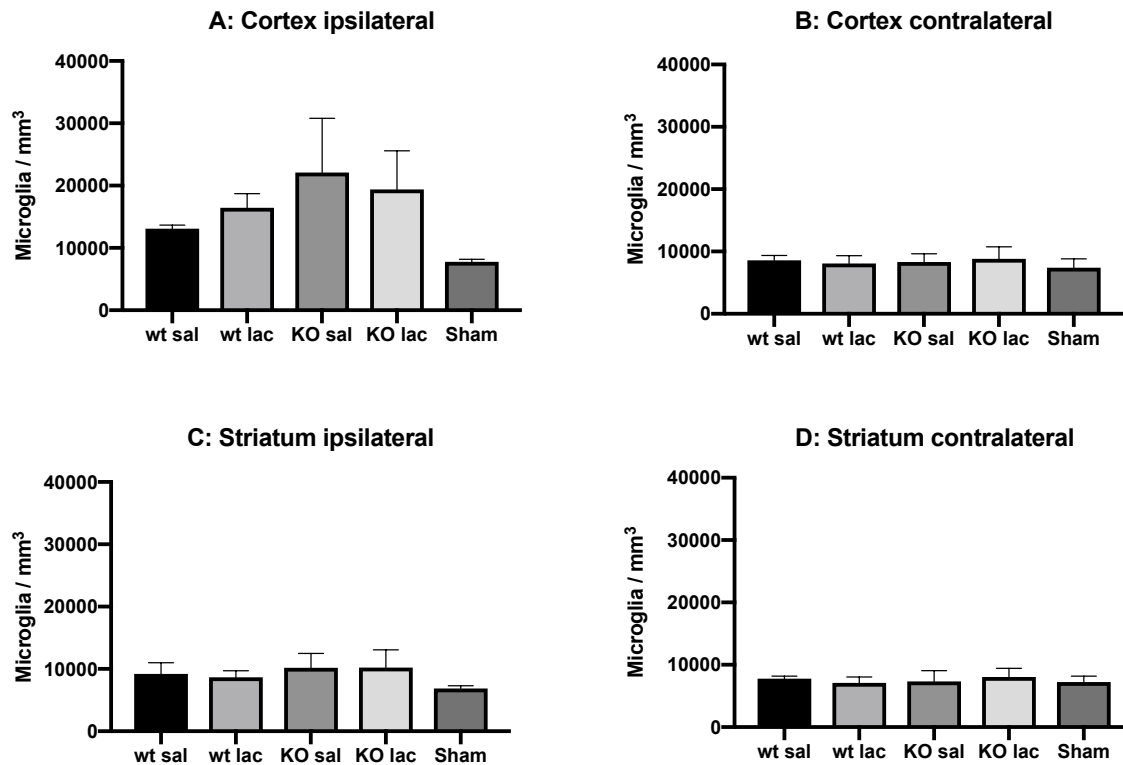
Figure 12 A: microglia density in the ipsilateral cortex of wild-type (wt) mice treated with saline (sal) (13,098 ± 579 microglia/mm^3, n = 3) and lactate (lac) (16,459 ± 2240 microglia/mm^3, n = 3), and HCAR 1 knock-out (KO) mice treated with sal (22,095 ± 8702 microglia/mm^3, n = 6) and lac (19391 ± 6200< microglia/mm^3, n = 6) (sham: 7415 ± 1415 microglia/mm^3, n = 3). **B:** microglia density in the contralateral cortex of wt mice treated with sal (8576 ± 785 microglia/mm^3, n = 3) and lac (8073 ± 1270 microglia/mm^3, n = 3), and HCAR 1 KO mice treated with sal (8301 ± 1324 microglia/mm^3, n = 6) and lac (8815 ± 1944 microglia/mm^3, n = 6) (sham: 7415 ± 1415 microglia/mm^3, n = 3). **C:** microglia density in the ipsilateral striatum of wt mice treated with sal (9217 ± 1792 microglia/mm^3, n = 3) and lac (8650 ± 1062 microglia/mm^3, n = 3), and HCAR 1 KO mice treated with sal (10177 ± 2320 microglia/mm^3, n = 6) and lac (10236 ± 2823 microglia/mm^3, n = 6) (sham: 6861 ± 453 microglia/mm^3, n = 3). **D:** Microglia density in the contralateral striatum of wt mice treated with sal (7770 ± 410 microglia/mm^3, n = 3) and lac (7103 ± 943 microglia/mm^3, n = 3), and HCAR 1 KO mice treated with sal (7338 ± 1730 microglia/mm^3, n = 6) and lac (8028 ± 1389 microglia/mm^3, n = 6) (sham: 7207 ± 943 microglia/mm^3, n = 3). There was no significant difference between the groups (one-way ANOVA, SPSS).

Furthermore, in all groups, the density of Iba1-postive cells were higher in the peri-lesional cortex than in the corresponding contralateral cortex (wt sal: 87% increase, p= 0.0012 (paired students t-test, Microsoft excel); wt lac 120% increase, p=9x10^{-6} (paired students t-test, Microsoft excel); KO sal: 163% increase, p=0.0003 (paired students t-test, Microsoft excel) for KO lac: 138% increase, p=0.0003 (paired students t-test, Microsoft excel)).

The ratio of microglia density in each hemisphere was also calculated to account for individual variation in innate microglia density. Despite the difference in % increase between groups reported above, the ratio of Iba1-positive cell densities in the ipsilateral versus contralateral cortex was unaffected by treatments and genotypes (p= 0.224, one way ANOVA, SPSS). In the striatum, the ratio of Iba1-positive cell densities in the ipsilateral

versus contralateral hemisphere was less than 35% in all groups. There were no significant differences in the Iba1-positive cell density ratio, but both lactate treated groups showed borderline significance (p=0.053 and p=0.052 in wt lac and KO lac, respectively, one-way ANOVA, SPSS) (figure 13).
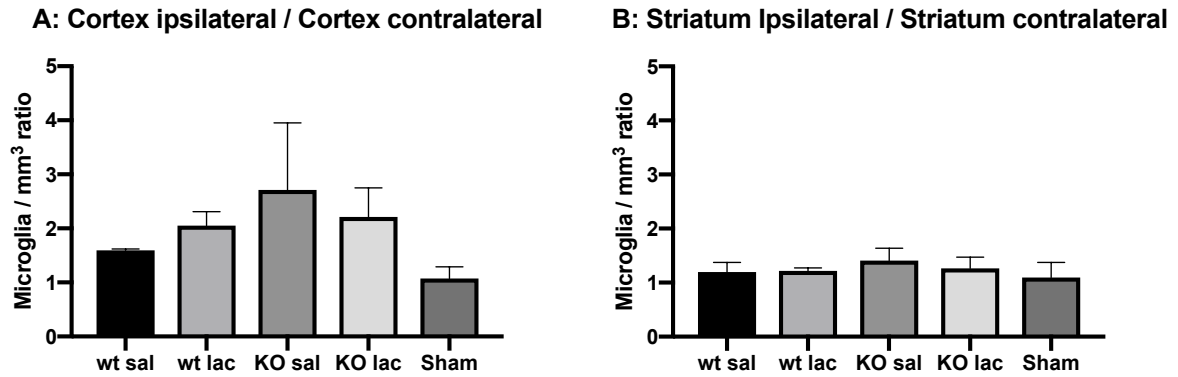
Figure 13 A: the microglia density ratio between the ipsilateral cortex and the contralateral cortex in wild-type (wt) mice treated with saline (sal) (1.595 ± 0.025, n = 3) and lactate (lac) (2.053 ± 0.259, n = 3), and HCAR1 knock-out (KO) mice treated with sal (2.711 ± 1.239, n = 6) and lac (2.212 ± 0.537, n = 6) (Sham: 1.073 ± 0.216, n = 3). **B**: the microglia density ratio between the ipsilateral striatum and the contralateral striatum in wt mice treated with sal (1.198 ± 0.177, n = 3) and lactate (lac) (1.219 ± 0.052, n = 3), and HCAR1 KO mice treated with sal (1.408 ± 0.229, n = 6) and lac (1.264 ± 0.205, n = 6) (sham: 1.095 ± 0.279, n = 3).

5 Discussion

5.1 Methodical discussion

5.1.1 Animals

As first described by Russell and Birch in 1959 (123), "the three Rs" for ethical use of animals in research (replacement, reduction and refinement) dictated that a thorough evaluation of non-animal substitutes should be conducted before animal models are applied. *In vitro* models will always be received as a more ethical alternative. It provides fewer variables than *in vivo* models, which in early stages of research may be beneficial. In light of recent progression in the research of HCAR1s possible neuroprotective and neurorestorative properties, *in vitro* models were deemed insufficient to adequately resemble the highly heterogeneous conditions of a focal ischaemic stroke. The use of animal models was considered the next necessary step on the road to a possible clinical application in humans.

Traditionally, mice have been widely used in medical and biological research for a number of reasons (124). They are relatively easy to house, with short generation time and life expectancy. Mice are also less-sentient mammalian species, meaning they are considered more ethically sound to use as animal models than other phylogenetic human relatives. In order to provide significant findings, stroke models should be kept simplistic and easily reproducible. On the other hand, the very illness they mimic are highly heterogeneous and no instance is the same in clinical practise (125). Which findings are transferable to human biology may not be reviled before the principle is put through clinical testing. As the translational gap between research in stroke models and clinical application may seem long, it is important not to undermine the advances that would not be possible without the use of animal research models.

5.1.2 Lactate administration and kinetics

Lac mice were treated with 2 g/kg i.p. sodium L-lactate 24 and 48 hours after the occlusion procedure. In a similar study, plasma lactate levels was observed to reach a C_{max} of that was close to fivefold the baseline concentration after approximately 15 minutes (T_{max}) (126). The concentration gradually decreased and reached a concentration that was twofold the baseline after one hour. After three hours the plasma concentration was normalised. In comparison, the same study observed 150% in lactate plasma concentration from baseline immediately

after a 42 minute run at 18 m/min (no elevation). Another study observed plasma lactate concentrations in mice after 30 minutes of intense exercise (forced run at 30 m/min, 30 degree incline) reach levels close to 10 mM, although the reliability of these methods are being discussed (127). In freely moving rats, the hippocampal lac concentration increased by 56% (to ~ 2 mM) in response to serum lac concentration being titrated to 9.5 mM (43). In the brain, HCAR1 is most intensely expressed in pericytes and fibroblasts lining the cerebral vasculature (29), where the lac exposure could be expected to be higher than in the hippocampus when the serum concentration is increased. When considering that the EC_{50} of L-lactate acting on HCAR1 is currently estimated to be in the range of 1-5 mM, 2 g/kg i.p. injections should yield a close to complete HCAR1 activation for at least one hour.

5.1.3 Occlusion

The perminant distal MCAO moddel was chosen based on several factors. As for the location of the occlusion, proximal MCAO models generally yeild larger infarcs which affects subcortical structures (for review see Carmichael, 2005 (107) and Canazza et al., 2014 (109)). This may in turn result in a wider array of complications (e.g. hypothermia) and is more ethically demanding. In addition, subcortical structures (hippocampus and ventricular sones) were of interest in other parts of the study. Transient MCAO models are generaly more intricate and time consuming which in turn inctreases the workload, anestesia exposure for the animals, and risk of complications (e.g. subarachnoid hemmorage and eodema). The unintended death rate is lower among distal MCAO models, which is favorable in reguards to the aforementioned three R´s. Thromboembolic methods are widely used and may closely mimic a naturally occurring stroke, but are limited by variability in lesion development.

Permanent electrocoagulation of the distal MCA can be performed with high accuracy and yield reproducible infarct lesions. The main disadvantage is the demand for surgical craniectomy, which requires expertise and may carry some risk for the animals. Arguably, transient MCAO would reflect a different pathological picture, especially when considering post-ischemic events (e.g. inflammation and oxidative stress). On the other hand, not all occluded arteries are successfully recanalised in clinical practise, and patients that does not receive thrombolysis or thrombectomy may be more in need of neurorestorative therapy. The photothrombosis model can also be aimed at the distal MCA and does not require craniectomy (128). By injecting a photosensitive dye (e.g. rose-bengal) and subsequently

radiating of the artery of interest (through the skull), endothelial damage and platelet activation causes microvascular occlusion throughout the irradiated area. Disadvantages include: small ischaemic penumbra caused by the widespread microvascular occlusion and the resultant abcense of collateral flow, and an increased occurance of brain eodema. As the penumbra was of interest in the precent study and edema would be of disturbance to the lesion volume measurements, the photothrombosis model was deemed unfavorable.

5.1.4 Fixation

As discussed, perfusion fixation (*in vivo* fixation) was considered necessary due to the hypoxic intolerance of the nervous tissues. The alternative, immersion fixation, involves dissecting the tissue of interest out of the animal and immersing it in a fixative solution (129). Larger tissue samples may be heterogeneously fixed, as the core of the tissue will be exposed to less fixative than the periphery (116). There has also been demonstrated an increase in hemispheric volume from immersion fixation compared to perfusion fixation (130). In the present study, the requirement for serial sectioning for volumetric analysis, dictated the need to fix the brains as one piece. For this reason immersion fixation was ruled unsuited due to the possible hypoxic effects and the size of tissue. Instead, perfusion of the fixative through the circulatory system yields a more homogenous fixation, and ensures penetration of fixative to all parts of the tissue

On deciding what cross-linking fixative to use, in what concentration and time of duration, a compromise must be made between morphological conservation and epitope availability for subsequent immunolabeling. An alternative fixative to FA is glutaraldehyde (GA). GA has two aldehyde groups separated by three methylene bridges (114, 116). These properties result in higher cross-linking activity, which to a larger extent preserves the tissues cytoarchitecture, but reduces the antigenicity by "masking" epitopes, which may prove difficult to overcome with antigen retrieval techniques. These aspects makes GA fixation ideal for electron microscopy, when immunolabeling is not required. Due to its low molecular weight, FA penetrates tissues faster than GA, which contributes to a more homogenously fixed tissue with less hypoxic damage (114). GA and FA may be used in combination, however, GA produces autofluorescence, which might have precluded the immunofuorescent experiments of the present study. An obvious disadvantage of cross-

linking fixatives is the high toxicity, which demands great care when the fixatives solutions are prepared, used and discarded.

5.1.5 Cryoprotection and sectioning

Cryoprotection

Prior to sectioning, cryoprotection of the tissue was insured by immersing the brains in 30% sucrose solution with 0.1 M NaPi over night. Intracellular water will normally expand and crystallize when the tissue is being frozen, causing cellular damage. Hypertonic sucrose will extract most of the water from the cells by exosmosis, thereby preventing damage to the cells when the temperature is rapidly reduced from room temperature to -20 °C and lower.

Sectioning

The fixed and cryoprotected brains were serial sectioned with sliding microtomes, equipped with a static tissue plate capable of freezing the tissues, and a sliding steel knife. These microtomes are easy to operate and ideal for cutting sections > 10 μm from fixed tissue, which allowed for sections to be stored in buffered solution for subsequent mounting or immunolabeling (131). The brains where frozen and moulded in frozen sucrose solution in order to preserve the tissues structural integrity during the sectioning. The ideal temperature for cryosectioning will depend on the tissues composition (amounts of water and lipids). Too high or low temperature may cause curling or rifting of the sections. Experience indicated that -20 °C was ideal for FA fixed mouse brains.

Cryostat sectioning is normally combined immediate mounting of all sections (131). This was ruled inexpedient, as the measurement of lesion volume only required every 8th section to be mounted and immunolabeling was performed only on selected sections from each brain. The rocking microtome (also known as the Cambridge rocking microtome) was also ruled unsuited as it produces curved sections, which would be inconvenient for volumetric measurements.

The main obstacle of the sliding microtome is to make sure that the brain is placed completely vertical on the ice stage. Brains placed with a tilt will result in oblique sections, which may interfere with subsequent analyses of the tissue. It should be mentioned that this problem is not exclusive for the sliding microtome.

5.1.6 Staining

Fixed tissue sections are colourless and staining was necessary in order to distinguish anatomical structures. At first, haematoxylin and eosin (H&E) staining was tested. In H&E staining, haematoxylin stains anionic cellular components (e.g. nucleus), while eosin stains cationic structures (e.g. proteins) (118). This method generally yields dark, haematoxylin stained nuclei, outlined by pink, eosin stained cytoplasm and extracellular matter. Unfortunately, H&E resulted in unevenly stained sections, which would make morphological analyses difficult. When comprehensive trouble-shooting did not suffice, nissl staining was introduced as a substitute for H&E. Nissl staining is generally performed with a single cationic dye (cresyl violet/blue) without any counterstain (118). It is commonly used for examination of neuronal tissue, and yielded consistent results as opposed to H&E. Microscope inspection verified that the healthy and ischaemic tissues was easily distinguishable without any counterstain.

Another alternative is the immersion of fresh, unfixed sections in 2,3,5-triphenyltetrazolium (TTC), which is oxidised to a dark red precipitate in the presence of normal concentrations of dehydrogenases i.e. in healthy tissue (132). The method was proved to be an inexpensive and reliable method for infarction detection, but was deemed inexpedient as other experiments that were to be performed required fixed tissue sections.

5.1.7 Volumetric measurement of stroke lesion

Due to some technical and procedural inconsistencies, a small percentage of the brains were sectioned at ether 40 μm, 30 μm. These inconsistencies where noted and corrected during the calculation of lesion volume.

The number of included sections from each brain varied (between 24 and 29 for brains sectioned at 20 μm). This might be due to the use of anatomical structures (corpus callosum and the hippocampus) to determine what sections where within the predetermined bregma coordinates that was to be quantified (1.5 mm rostral and 2.5 mm dorsal of bregma). Hemispheric lateral asymmetries have been described in humans as well as inbred or genetically altered rodents (133). The hippocampus in particular has been demonstrated to be subject of lateral asymmetry with evidence suggesting that the left hippocampus is relatively larger than the right. Alterations caused by fixation, atrophy or artefacts from the

cryosectioning may also have contributed to the variations in distance between the anatomical structures. This may also be the reason for the mean number of sections included from each brain (27.1 for the 20 μm section brains) being more than the theoretical number sections:

$$Theoretical\ number\ of\ sections = \frac{4000\ \mu m}{160\ \mu m} = 25$$

If the number sections (n) within the predetermined bregma coordinates was consistently in correlation with the theoretical number of sections (n = 25), the lesion volume (LV) could be calculated by simply summarising the difference in cortical area multiplied by 160 μm in each section. One would thereby assume that the distance of the intervals between the sections is true, and the variation is due to inconsistencies in the distance between the anatomical structures that where used as markers of the predetermined bregma coordinates:

$$LV = \sum_{k=1}^{n} \left((CCA - ICA) \times 160\ \mu m \right)_k$$

The variance necessitated an adjusted recalculation of LV (LVa) where the intervals between the sections were redetermined under the assumption of the distance between the anatomical markers of bregma coordinates (4 mm) was true:

$$LVa = \sum_{k=1}^{n} \left((CCA - ICA) \times \frac{4\ mm}{n} \right)_k$$

The distance interval between included sections were determined based on intervals used in similar studies of stroke models in mice, which generally ranges from 400 μm (106, 134) to 2000 μm intervals (135) for 20 μm sections. Swanson et al. demonstrated that intervals ranging from 200 μm to 740 μm yield nearly identical infarct volume values (119). Nevertheless, a test was performed by comparing lesion volume measured with 160 and 320 μm intervals. There were more variations in measurments made with 320 μm, which led to 160 μm intervals being implemented.

Measurements were made manually and distinguishment between healthy and lesioned tissue was based on visual cues. Correct recognition of anatomical structures where ensured by comparing the sections with a coronal mouse brain atlas (Allen Mouse Brain Atlas - https://mouse.brain-map.org/experiment/thumbnails/100048576?image_type=atlas). To ensure reproducibility, two independent technicians measured a sample of brains. The compared results demonstrated good inter-observer agreement.

5.1.8 Immunohistochemistry

Quantitation of microglia was performed on brains extracted at one week after distal MCAO, based on data indicating that microglia activation peaks within the first week after ischaemic brain injury in mice (136, 137).

Monoclonal versus polyclonal antibodies

Antibodies (Abs,) also known as immunoglobulines, are glycoproteins secreted by plasma cells (differentiated from activated B lymphocytes) (138, 139). They share a common Y-shaped structure. The two "arms" are referred to as the fragment antigen binding (Fab) region and the "base" is called the fragment crystallisable (Fc) region. The Fab region contains antigen-binding domains, which are made highly heterogeneous through several mechanisms by the plasma cells in order to recognise a large array of antigens. Polyclonal Abs (PAbs) are secreted from several plasma cell clones and collectively targets several epitopes on the same antigen. Monoclonal Abs (MAbs) are secreted from a single plasma cell clone and therefore targets only one epitope. These properties precipitate different practical qualities. An Ab´s specificity refers to it´s ability to recognize specific epitopes (138). Hence, unspecific recognition refers to various degrees of unintended epitope recognition. The monospecificity of MAbs will ideally yield highly specific immunolabeling, but renders them vulnerable to irregularities in the target epitope. Such irregularities may result from glycosylation, denaturation, and, *ad rem*, conjugating fixatives. Physical and chemical instabilities may also have a greater impact on the functionality of MAbs because of the homogeneous conformation of the antigen binding domains. Polyclonal Abs (PAbs) will recognize several epitopes and are therefore more resistant to variations in some of the target antigens epitopes. PAbs polyspecificity gives a higher probability for off-target effects and unspecific

48

background labeling, although the latter is often unproblematic due to implementation of blocking procedures. In the present study, PAbs were used for IHC purposes.

Validation

The quality of Abs may fluctuate and be batch specific, which may call for preliminary validation of any new Abs or new batch of previously used Abs (140). Western blotting is often performed for this purpose, although it will only be indicative for other IHC methods and require homogenate and a molecular weight marker. It is also generally not recommended to perform Western blots on FA fixed tissue, as cross-linking will hinder the denaturation of tertiary and quaternary structure. The use of blocking peptides is a more suited validation method for Abs intended for IHC on FA fixed tissue (140). Abbreviated, the method is performed by incubating the Abs with a blocking peptide in great excess. The blocking peptide is the same sequences used to generate the antibody. Tissue known to express the target antigen is then stained with ABs incubated with blocking peptides and compared to tissue stained with unblocked Abs. The result should be no detectable staining by the blocked Abs compared to unblocked Abs. The ideal validation method is to perform IHC on tissue or cell lines known not to express the target antigen (e.g. KO), although it is often expensive and/or time consuming (140). Prior to the present study, the Iba1 Abs from rabbit had been validated through extensive use with consistent and reliable results. Since Iba1 Abs were used to recognize microglia, as opposed to demonstrating Iba1 presence in these cells, the labeling could be verified by comparing the labeling to the known microglia morphology published in the literature.

Colorimetric vs. fluorescent immunohistochemistry

Colorimetric IHC is generally considered to be best suited for qualitative assays, as the staining results from an enzymatic reaction (120). The degree of staining will therefore be determined by the availability of substrate and physical space for the enzymatic product to be deposited, and not only the presence of the antigen in question, as in fluorescent IHC.

5.2 General discussion of the findings

5.2.1 The correlation between HCAR1, lactate and lesion volume

The results from the measurement of lesion volumes are ambiguous. The volumes measured one week after permanent distal MCAO, display no reliable significant correlation between the different genotypes or treatment groups (figure 6). The volumes measured in brains three weeks after the permanent distal MCAO display different picture (figure 8). The fact that the significantly lower average lesion volume in the wt lac group compared to the wt control group was not replicated among the KO groups indicates a HCAR1 dependent lesion volume reducing effect of lactate, three weeks after stroke. The recently discovered HCAR1-dependent, lactate mediated increase in cerebral capillary density (se above) and the logical notion that this would be beneficial to the neurological outcome of cerebral stroke is not consistently reflected in the results, as the average lesion in the KO sal groups volume is, although insignificantly (one week: $p = 0.528$, three weeks: $p = 0.059$, one-way ANOVA, Tukey´s post hoc test, SPSS) smaller than the corresponding wt sal groups after one and three weeks (figure 6, figure 8). It could be speculated that the KO mice, through the absence of HCAR1, developed a compensatory phenotype that does not rely on lactate (for review of compensatory mechanisms in KO research animals, see: Mohammad and Didier, 2017 (141)). In that case, the wt mice would be inherently more dependent on lactate for the neuroprotective effect exhibited by the significant difference in average lesion volume between the wt sal and the wt lac group after three weeks (figure 8). In addition, the HCAR1-mediated effects may not be detectable during the first week and require more time before the effects becomes significant.

When comparing the average lesion volumes at one and three weeks, there is little consistency nether within the individual groups, nor in the differences between the groups. One possible explanation is that areas that at one week histologically resembled infarcted tissue, in fact was penumbra (salvageable tissue) that after three weeks was restored to normal physiological tissue in some groups. When the stroke size was measured in animals one week after stroke induction, all tissue that did not look completely healthy was considered as lesioned. As mentioned, after one week the lesions where clearly visible and bordered corpus callosum for large extents of the barrel cortex (figure 5). In contrast, at three weeks, the lesions where mainly detected as a vague crater and thinning of the ipsilateral

cortex, in addition to occasional scar tissue (figure 7). This might be because parts of the penumbra were restored, and what was detected as the lesion was the remains of the ischaemic core. Summarised: At one week, the penumbra and the ischaemic core was considered infarcted tissue, at three weeks, only the ischaemic core (or the glial scar) was considered infarcted. Retrospectively, an apoptosis or necrosis assay of the infarcted tissue at one week could have produced some interesting insight on this issue. For instance, a terminal deoxynucleotidyl transferase deoxyuride triphosphate nick end labeling (TUNEL) assay, first implemented by Gavrieli et al., 1992 (142), could have been performed in order to distinguish the necrotic and apoptotic parts of the infarcted tissue at one week. The method is performed by using terminal deoxynucleotidyl transferase to catalyse the labeling of 3′-hydroxyl termini of DNA single or double strand breaks, an indication of apoptotic activity, with flourophore-conjugated deoxynucleotides (143). It should be noted that the integrity of apoptosis or necrosis assays used alone is under some debate as the markers (e.g. 3′-hydroxyl termini of DNA and cytochrome c release) may be absent or overlap with, yielding false positives and negatives (for review, see Zille et al., 2011 (144)). In some methods, this is issue may to a certain extent be accounted for by combining markers for necrosis and apoptosis.

An obvious point to detail is the low number of individuals, especially in the wt groups. The lack of mice in these groups was mainly due to unfortunate events, likely unrelated to the procedure (see above). As a consequence, the results from these groups are tainted with uncertainty. For instance, there was no significant difference between the average lesion volumes in the wt sal groups at one and three weeks after stroke induction ($p = 0.4542$, paired students t-test, Microsoft excel) as opposed to all other treatment groups (wt lac: $p = 0.0117$, KO sal: $p = 0.0003$, KO lac: $p = 0.0121$, paired students t-test, Microsoft excel). It could be speculated that the average lesion volume in the wt sal group at three weeks was affected by low number of individuals in the groups. The fact that the number of sections and the intervals they were spaced at did not consistently correlate with the theoretical distance of the predetermined bregma coordinates is indicative of some methodical room for improvement. It is also dubious which results to rely on, the unadjusted (the distance of the section intervals is assumed to be true) or the adjusted (the distance between bregma coordinates is assumed to be true). In the sham operated mice, a difference in cortical volume of about $\sim 2 \text{ mm}^3$ was detected ($1.95 \text{ mm}^3 \pm 0.97 \text{ mm}^3$), although there were no histological signs of infarct. This might be the result of naturally occurring lateral asymmetry (133), or be the effects of

atrophy from the craniectomy, perfusion fixation or artefacts from the sectioning. There were also occasional sections affected by artefacts witnessing ether temperature irregularities during sectioning or improper fixation. As mentioned, when choosing fixative and fixation method, a compromise must be made between structural integrity and epitope availability. On the other hand, the average lesion volumes one and three weeks after permanent distal MCAO correlates with average lesion volumes reported in similar studies ($15.4 \pm \sim 1.5$ mm^3 after one week, reported by Llovera G. et al., (106), and 14.5 ± 5.7 mm^3 after three weeks, reported by Freret et al., (145)). This correlation indicates that the results are comparative to similar studies on the matter. Nevertheless, increasing the number of animals in each group to at least six would greatly increase the credibility of the results.

5.2.2 The correlation between HCAR1, lactate and post stroke microglia proliferation and recruitment

There were no significant differences when the microglia densities in the isolated areas of interest were compared (figure 12). It should be noted that the wt mice generally had a lower average density than the KO mice, especially in the ipsilateral cortex. As the wt sal group had the lowest microglial density in the ipsilateral cortex after one week, the microglia density and the degree of inflammation it reflects cannot be applied as a possible explanation for the unexpectedly similar average lesion volumes one and three weeks after stroke induction (figure 8, figure 12). On the basis of these findings, it cannot be concluded that lactate has any modulating effect on the migration and proliferation of microglia in the perilesional tissues or the corresponding contralateral tissues one week after focal ischaemic stroke. It may also be interpreted as an indirect indication that lactate does not affect the degree of inflammation in the penumbra, and the lesion reducing effect detected three weeks after stroke induction is the result of a process unrelated to microglia activation and proliferation.

Once again, the integrity of the results must be considered to be somewhat affected by the low amount of individuals in the wt groups (see above). In fact, even more so as one wt sal sample and one HCAR1 KO lac were lost during the IHC procedure.

Physiological microglia densities varies between the different structures of the adult mouse brain (for review, see Keller et al., 2018 (146)). The density is estimated to be ~ 6500 microglia/mm^3 in the cortex (147, 148), and between 9700 (148) - 15000 (149)

microglia/mm^3 in the striatum. In the sham-operated animals, the average cortical microglia density (7588 ± 953 microglia/mm^3) could be said to be in some correlation with what has previously been reported. In the striatum, the average density (6774 ± 582 microglia/mm^3) was somewhat lower than what has been previously observed, although it should be noted that both the striatum and cortex are large cerebral structures, and some interstrucural variance should be expected as well as variance among different strains of research mice. Different quantitation methods may also cause some variation amongst the reported densities. Quantitation of microglia density in the penumbra after focal ischaemic stroke is somewhat unexplored as a method for comparison of post-stroke-inflammation. In response to other injurious stimuli (for instance systemic lipopolysaccharide (LPS) injection), the proliferating response of microglia is well documented (150, 151). Of the few comparable values reported, one could expect a density between ~ 11,000 (observed in the penumbra, 7 days after a 60 minutes transient MCAO in mice by Barreto et al., 2011 (152)) and ~ 40,000 microglia/mm^3 (observed seven days after photothrombotic occlusion in the somatosensory cortex in mice by Li et al. 2013 (153)) in the cortical penumbra, seven days after focal ischemic stroke in mice. The densities recorded in penumbra (ipsilateral cortex: 13,098 ± 579 microglia/mm^3) correlates with what has been previously observed under similar circumstances. The significant linear relationship between lesion volume and microglia density in both the ipsilateral cortex and striatum (figure 11, ipsilateral cortex: p = 0.016, ipsilateral striatum: p = 0.041, linear regression, GraphPad) corroborate the measurement of microglia density as an indication of neuronal damage after stroke.

Analyses of the microglia morphology would have been an interesting addition to the perspective of the present study, as microglia density alone may be perceived as a somewhat narrow marker for degree of inflammation. Methods have been described where the stages of activation has been analysed based on morphology (e.g. length, thickness, and branching of processes and size of the soma) both manually and digitally. Different morphological characteristics have been associated with different degrees of microglia activation and have been used to quantify the degree of activation within the analysed tissue (e.g. Sholls analysis) both with colorimetric and fluorescent IHC (151, 154). In addition, Abs selective for the different activated microglia phenotypes (M1 and M2) has also been described and utilised in fluorescent ICH with subsequent confocal microscopy analyses in order to quantify the state of differentiation of microglia under different circumstances (for review, see Patel et al., 2013 (155)). As the different phenotypes has been associated with different degree of neuronal

damage, a quantification of expression of the different phenotypes would have been an interesting insight, especially in comparison with the lesion volumes. Unfortunately, this was unachievable due to limitations in time and available recourses.

6 Conclusion

Lactate has a beneficial effect on the development of infarct lesions caused by focal ischaemic stroke. In the present study, an HCAR1-dependent lesion-reducing effect of lactate was detected three weeks after permanent occlusion of the distal MCA, but not after one week. No significant effect of lactate (neither HCAR1-dependent nor independent) on the microglia density in the affected tissue could be detected one week after stroke. As the lesion reducing effect becomes significant between one and three weeks after stroke induction, a study where lesion volumes are measured at a more frequent rate would be beneficial in order to better understand the development over time. In addition, more data is required to determine if lactate has a modulating effect on inflammation in the stroke-affected brain. Studies where more direct indicators of inflammation in addition to microglia mortphology and phenotypes are quantified would be valuable to further determine if modulation of inflammatory processes is involved in the neuroprotective effect of lactate after focal ischaemic stroke.

Appendix A - Chemicals and reagents

Product	Manufacturer
3,3-diaminobezidine (DAB)	Sigma-Aldrich, USA
4,6-diamidino-2-phenylindole (DAPI)	Sigma-Aldrich, Israel
Acetic acid (glacial) 100%	Merck, Germany
Biotin-streptavidin-HRP	Thermo Fisher Scientific, USA
Bovine serum albumin (BSA)	Sigma-Aldrich, USA
Cresyl violet acetate	Sigma-Aldrich, USA
Di-Sodium hydrogen phosphate dehydrate	Merck, Germany
Ethanol	Antibac, Norway
Glycerine-gelatine	Sigma-Aldrich, USA
Newborn calf serum (NCS)	Invitrogen, USA
Hydrogen Peroxide (H_2O_2)	Sigma-Aldrich, USA
Neo-Mount®	Merck, Germany
Neo-Clear	Merck, Germany
Paraformaldehyde (PFA)	Sigma-Aldrich, USA
Potassium chloride	Merck, Germany
Potassium dihydrogen phosphate	Merck, Germany
ProLong Gold	Invitrogen, USA
Sodium azide	Sigma-Aldrich, USA
Sodium chloride	VWR Chemicals, Belgium
Sucrose	Merck, Germany
Trisodium citrate dihydrate	Sigma-Aldrich, Belgium
Triton X-100	Sigma-Aldrich, USA

Appendix B - Antibodies

Primary antibodies			
Target antigen	Host species	Catalogue number	Manufacturer
Iba1	Rabbit	019-19741	Wako, USA

Secondary antibodies				
Antibody	Target species	Host species	Catalogue number	Manufacturer
Alexa Fluor 488	Rabbit	Donkey	A21206	Invitrogen, USA
Horseradish Peroxidase IgG	Rabbit	Goat	G21234	Invitrogen, USA

Appendix C - Equipment

Equipment	Manufacturer
Automatic surface scanning hardware; SteREO Lumar V12	Carl Zeiss Microscopy, Germany
Confocal microscope; Zeiss LSM880 - Fast Airy Scan	Carl Zeiss Microscopy, Germany
Drill, rotary	Dremel, USA
Glass slides; Superfrost Pluss	Thermo Fisher Scientific, USA
High-frequency generator; VIO 50C	Erbe, USA
Laboratory film; Parafilm M	Thermo Fisher Scientific, USA
Light microscope; Zeiss Axio Scan Z1	Carl Zeiss Microscopy, Germany
Multipipette; Multipipette® pluss	Eppendorf , Germany
Paintbrush; 0.3 and 0.1 mm pine marten	Panduro Hobby, Sweden
Peristaltic pump; Watson Marlow 323	Watson Marlow, UK
Sliding microtome; HM 450	Thermo Fisher Scientific, USA
Well plates; Nunclon 24-well cell culture plates	Thermo Fisher Scientific, USA
Well plates; Tissue culture plates, 12 wells sterile	VWR, USA

References

1. Katan M, Luft A. Global Burden of Stroke. 2018;38(02):208-11.
2. Krishnamurthi RV, Feigin VL, Forouzanfar MH, Mensah GA, Connor M, Bennett DA, et al. Global and regional burden of first-ever ischaemic and haemorrhagic stroke during 1990–2010: findings from the Global Burden of Disease Study 2010. The Lancet Global Health. 2013;1(5):e259-e81.
3. Correction to: Heart Disease and Stroke Statistics—2018 Update: A Report From the American Heart Association. Circulation. 2018;137(12):e493-e.
4. Murray CJL, Atkinson C, Bhalla K, Birbeck G, Burstein R, Chou D, et al. The state of US health, 1990-2010: burden of diseases, injuries, and risk factors. 2013. p. 591-608.
5. National Library of M. Prevalence and most common causes of disability among adults--United States, 2005. 2009. p. 421-6.
6. Fang J, Shaw K, George M. Prevalence of Stroke-United States, 2006-2010. JAMA. 2012;308(3):228.
7. Koton S, Schneider ALC, Rosamond WD, Shahar E, Sang Y, Gottesman RF, et al. Stroke Incidence and Mortality Trends in US Communities, 1987 to 2011. JAMA. 2014;312(3):259-68.
8. Auer RN. 4 - Histopathology of Brain Tissue Response to Stroke and Injury: Elsevier Inc.; 2016. 47-59 p.
9. Chrissobolis S, Sobey CG. 1 - Vascular Biology and Atherosclerosis of Cerebral Vessels: Elsevier Inc.; 2016. 3-12 p.
10. Dirnagl U, Iadecola C, Moskowitz MA. Pathobiology of ischaemic stroke: an integrated view. Trends in Neurosciences. 1999;22(9):391-7.
11. Adams HP, Bendixen BH, Kappelle LJ, Biller J, Love BB, Gordon DL, et al. Classification of subtype of acute ischemic stroke. Definitions for use in a multicenter clinical trial. TOAST. Trial of Org 10172 in Acute Stroke Treatment. 1993. p. 35-41.
12. Grau JA, Weimar JC, Buggle JF, Heinrich JA, Goertler JM, Neumaier JS, et al. Risk Factors, Outcome, and Treatment in Subtypes of Ischemic Stroke: The German Stroke Data Bank. Stroke: Journal of the American Heart Association. 2001;32(11):2559-66.
13. Mink JW, Blumenschine RJ, Adams DB. Ratio of central nervous system to body metabolism in vertebrates: its constancy and functional basis. American Journal of Physiology-Regulatory, Integrative and Comparative Physiology. 1981;241(3):R203-R12.
14. Rolfe DF, Brown GC, Rolfe DF. Cellular energy utilization and molecular origin of standard metabolic rate in mammals. Physiological reviews. 1997;77(3):731-58.
15. Powers WJ. Cerebral Blood Flow and Metabolism: Regulation and Pathophysiology in Cerebrovascular Disease. Stroke. 6: Elsevier Inc.; 2016. p. 28-46.
16. Cheng J, Korte N, Nortley R, Sethi H, Tang Y, Attwell D. Targeting pericytes for therapeutic approaches to neurological disorders. Pathology and Mechanisms of Neurological Disease. 2018;136(4):507-23.
17. Powers WJ. Cerebral hemodynamics in ischemic cerebrovascular disease. Annals of Neurology. 1991;29(3):231-40.
18. Obermeier B, Daneman R, Ransohoff RM, Obermeier B. Development, maintenance and disruption of the blood-brain barrier. 2013. p. 1584-96.
19. Engelhardt B, Sorokin L. The blood–brain and the blood–cerebrospinal fluid barriers: function and dysfunction. Seminars in Immunopathology. 2009;31(4):497-511.
20. Abbott NJ, Rönnbäck L, Hansson E, Abbott NJ. Astrocyte-endothelial interactions at the blood-brain barrier. 2006. p. 41-53.

21.   Richard MR, Britta E. The anatomical and cellular basis of immune surveillance in the central nervous system. Nature Reviews Immunology. 2012;12(9):623.

22.   Pierre JM, Igor A. Lactate in the brain: from metabolic end-product to signalling molecule. Nature Reviews Neuroscience. 2018;19(4):235.

23.   Pellerin L, Magistretti PJ, Pellerin L. Glutamate uptake into astrocytes stimulates aerobic glycolysis: a mechanism coupling neuronal activity to glucose utilization. Proceedings of the National Academy of Sciences of the United States of America. 1994;91(22):10625-9.

24.   Hamberger A, Hyden H. Inverse enzymatic changes in neurons and glia during increased function and hypoxia. 1963. p. 521.

25.   Lopez-Fabuel I, Le Douce J, Logan A, James AM, Bonvento G, Murphy MP, et al. Complex I assembly into supercomplexes determines differential mitochondrial ROS production in neurons and astrocytes. Proceedings of the National Academy of Sciences. 2016;113(46):13063-8.

26.   Pierre K, Pellerin L. Monocarboxylate transporters in the central nervous system: distribution, regulation and function. Oxford, UK2005. p. 1-14.

27.   Newman LA, Brann D, Korol DL, Gold PE, Brann D. Lactate Produced by Glycogenolysis in Astrocytes Regulates Memory Processing. 2011. p. e28427.

28.   Sotelo-Hitschfeld T, Niemeyer MI, Mächler P, Ruminot I, Lerchundi R, Wyss MT, et al. Channel-mediated lactate release by K$^+$-stimulated astrocytes. 2015. p. 4168-78.

29.   Morland C, Lauritzen KH, Puchades M, Holm-Hansen S, Andersson K, Gjedde A, et al. The lactate receptor, G-protein-coupled receptor 81/hydroxycarboxylic acid receptor 1: Expression and action in brain. 2015. p. 1045-55.

30.   Lee DK, Nguyen T, Lynch KR, Cheng R, Vanti WB, Arkhitko O, et al. Discovery and mapping of ten novel G protein-coupled receptor genes. Gene. 2001;275(1):83-91.

31.   Cai T-Q, Ren N, Jin L, Cheng K, Kash S, Chen R, et al. Role of GPR81 in lactate-mediated reduction of adipose lipolysis. Biochemical and Biophysical Research Communications. 2008;377(3):987-91.

32.   Lauritzen KH, Morland C, Puchades M, Holm-Hansen S, Hagelin EM, Lauritzen F, et al. Lactate Receptor Sites Link Neurotransmission, Neurovascular Coupling, and Brain Energy Metabolism. Cerebral Cortex. 2014;24(10):2784-95.

33.   Morland C, Andersson K, Haugen ØP, Hadzic A, Kleppa L, Gille A, et al. Exercise induces cerebral VEGF and angiogenesis via the lactate receptor HCAR1. 2017.

34.   Tang F, Lane S, Korsak A, Paton JFR, Gourine AV, Kasparov S, et al. Lactate-mediated glia-neuronal signalling in the mammalian brain. Nature Communications. 2014;5.

35.   Ferrara N. Vascular endothelial growth factor and the regulation of angiogenesis. Recent progress in hormone research. 2000;55:15.

36.   Rossi PD, Harde E, Dupuis JP, Martin L, Chounlamountri N, Bardin M, et al. A critical role for VEGF and VEGFR2 in NMDA receptor synaptic function and fear-related behavior. Molecular Psychiatry. 2016;21(12).

37.   Sørli M. HCAR1-dependent intracellular signaling in fibroblast. 2018.

38.   Trabold O, Wagner S, Wicke C, Scheuenstuhl H, Hussain MZ, Rosen N, et al. Lactate and oxygen constitute a fundamental regulatory mechanism in wound healing. Wound Repair and Regeneration. 2003;11(6):504-9.

39.   Porporato P, Payen V, Saedeleer C, Préat V, Thissen J-P, Feron O, et al. Lactate stimulates angiogenesis and accelerates the healing of superficial and ischemic wounds in mice. Angiogenesis. 2012;15(4):581-92.

40.   Berthet C, Castillo X, Magistretti PJ, Hirt L. New Evidence of Neuroprotection by Lactate after Transient Focal Cerebral Ischaemia: Extended Benefit after

Intracerebroventricular Injection and Efficacy of Intravenous Administration. Cerebrovascular Diseases. 2012;34(5-6):329-35.

41.   Zhou J, Liu T, Guo H, Cui H, Li P, Feng D, et al. Lactate potentiates angiogenesis and neurogenesis in experimental intracerebral hemorrhage. Experimental & Molecular Medicine. 2018;50(7):78.

42.   Agnati LF, Fuxe K, Zoli M, Ozini I, Toffano G, Ferraguti F. A correlation analysis of the regional distribution of central enkephalin and β-endorphin immunoreactive terminals and of opiate receptors in adult and old male rats. Evidence for the existence of two main types of communication in the central nervous system: the volume transmission and the wiring transmission. Acta Physiologica Scandinavica. 1986;128(2):201-7.

43.   Harada M, Okuda C, Sawa T, Murakami T. Cerebral Extracellular Glucose and Lactate Concentrations during and after Moderate Hypoxia in Glucose-and Saline-infused Rats. Anesthesiology. 1992;77(4):728-34.

44.   Wohleb ES, Fenn AM, Pacenta AM, Powell ND, Sheridan JF, Godbout JP, et al. Peripheral innate immune challenge exaggerated microglia activation, increased the number of inflammatory CNS macrophages, and prolonged social withdrawal in socially defeated mice. 2012. p. 1491-505.

45.   Lampron A, Elali A, Rivest S. Innate Immunity in the CNS: Redefining the Relationship between the CNS and Its Environment. Neuron. 2013;78(2):214-32.

46.   Hanamsagar R, Hanke ML, Kielian T. Toll-like receptor (TLR) and inflammasome actions in the central nervous system. Trends in Immunology. 2012;33(7):333-42.

47.   Soulet D, Rivest S. Microglia. Current Biology. 2008;18(12):R506-R8.

48.   Varnum M, Ikezu T. The Classification of Microglial Activation Phenotypes on Neurodegeneration and Regeneration in Alzheimer's Disease Brain. Archivum Immunologiae et Therapiae Experimentalis. 2012;60(4):251-66.

49.   Hu KX, Li KP, Guo KY, Wang KH, Leak KR, Chen KS, et al. Microglia/Macrophage Polarization Dynamics Reveal Novel Mechanism of Injury Expansion After Focal Cerebral Ischemia. Stroke. 2012;43(11):3063-70.

50.   Costantino I, Josef A. The immunology of stroke: from mechanisms to translation. Nature Medicine. 2011;17(7):796.

51.   Torres-Platas S, Comeau S, Rachalski A, Bo G, Cruceanu C, Turecki G, et al. Morphometric characterization of microglial phenotypes in human cerebral cortex. Journal of Neuroinflammation. 2014;11(1):12.

52.   Liu H, Leak RK, Hu X. Neurotransmitter receptors on microglia. BMJ Publishing Group Ltd; 2016. p. 52.

53.   Deininger MH, Meyermann R, Schluesener HJ. The allograft inflammatory factor-1 family of proteins. FEBS Letters. 2002;514(2-3):115-21.

54.   Ahmed Z, Shaw G, Sharma VP, Yang C, McGowan E, Dickson DW. Actin-binding Proteins Coronin-1a and IBA-1 are Effective Microglial Markers for Immunohistochemistry. Journal of Histochemistry & Cytochemistry. 2007;55(7):687-700.

55.   Engelhardt B, Ransohoff RM. Capture, crawl, cross: the T cell code to breach the blood–brain barriers. Trends in Immunology. 2012;33(12):579-89.

56.   Sheth SA, Jahan R, Gralla J, Pereira VM, Nogueira RG, Levy EI, et al. Time to endovascular reperfusion and degree of disability in acute stroke. Annals of Neurology. 2015;78(4):584-93.

57.   Saver LJ. Time Is Brain—Quantified. Stroke. 2006;37(1):263-6.

58.   Gjerstad L, Helseth E, Rootwelt T, Enström K. Nevrologi og nevrokirurgi : fra barn til voksen. 6. rev. utg. ed. Høvik: Vett & viten; 2014.

59.   Kroemer G, Galluzzi L, Vandenabeele P, Abrams J, Alnemri ES, Baehrecke EH, et al. Classification of cell death: recommendations of the Nomenclature Committee on Cell Death 2009. Cell Death and Differentiation. 2008;16(1):3.

60.   Yuan J, Lipinski M, Degterev A. Diversity in the Mechanisms of Neuronal Cell Death. Neuron. 2003;40(2):401-13.

61.   Bao Q, Shi Y, Bao Q. Apoptosome: a platform for the activation of initiator caspases. 2007. p. 56-65.

62.   Zhang J, Chan FK-M. Cell biology. RIPK3 takes another deadly turn. Science (New York, NY). 2014;343(6177):1322.

63.   Festjens N, Vanden Berghe T, Vandenabeele P. Necrosis, a well-orchestrated form of cell demise: Signalling cascades, important mediators and concomitant immune response. BBA - Bioenergetics. 2006;1757(9):1371-87.

64.   Szydlowska K, Tymianski M. Calcium, ischemia and excitotoxicity. Cell Calcium. 2010;47(2):122-9.

65.   Kristián T, Siesjö BK. Changes in ionic fluxes during cerebral ischaemia. International review of neurobiology. 1997;40:27.

66.   David JR, James DB, Claudia M. Astrocyte metabolism and signaling during brain ischemia. Nature Neuroscience. 2007;10(11):1377.

67.   Nicholls D, Attwell D. The release and uptake of excitatory amino acids. Trends in Pharmacological Sciences. 1990;11(11):462-8.

68.   Xiong Z-G, Zhu X-M, Chu X-P, Minami M, Hey J, Wei W-L, et al. Neuroprotection in Ischemia: Blocking Calcium-Permeable Acid-Sensing Ion Channels. Cell. 2004;118(6):687-98.

69.   Rainer W, Guy C, Frédéric B, Catherine H, Michel L. A proton-gated cation channel involved in acid-sensing. Nature. 1997;386(6621):173.

70.   Olena Y, Leonard AS, Mikael KS, Francois MA, Michael JW. Extracellular acidosis increases neuronal cell calcium by activating acid-sensing ion channel 1a. Proceedings of the National Academy of Sciences of the United States of America. 2004;101(17):6752.

71.   Chan PH. Role of Oxidants in Ischemic Brain Damage. Stroke A Journal of Cerebral Circulation. 1996;27(6):1124-9.

72.   Bergendi L, Beneš L, Ďuračková Z, Ferenčik M. Chemistry, physiology and pathology of free radicals. Life Sciences. 1999;65(18):1865-74.

73.   Allen CL, Bayraktutan U. Oxidative stress and its role in the pathogenesis of ischaemic stroke. Oxford, UK2009. p. 461-70.

74.   Turrens JF, Beconi M, Barilla J, Chavez UB, McCord JM. Mitochondrial generation of oxygen radicals during reoxygenation of ischemic tissues. Free radical research communications. 1991;12-13 Pt 2:681.

75.   Sanderson T, Reynolds C, Kumar R, Przyklenk K, Hüttemann M. Molecular Mechanisms of Ischemia–Reperfusion Injury in Brain: Pivotal Role of the Mitochondrial Membrane Potential in Reactive Oxygen Species Generation. Molecular Neurobiology. 2013;47(1):9-23.

76.   Brennan-Minnella AM, Shen Y, El-Benna J, Swanson RA. Phosphoinositide 3-kinase couples NMDA receptors to superoxide release in excitotoxic neuronal death. Cell Death and Disease. 2013;4(4):e580.

77.   Christian M, Jan MS, Konstantin P, Andreas M, Ulrich D. Central nervous system injury-induced immune deficiency syndrome. Nature Reviews Neuroscience. 2005;6(10):775.

78.   Simard JM, Kent TA, Chen M, Tarasov KV, Gerzanich V. Brain oedema in focal ischaemia: molecular pathophysiology and theoretical implications. Lancet Neurology. 2007;6(3):258-68.

79.   Krupinski MJ, Kaluza MJ, Kumar MP, Kumar MS, Wang MJ. Role of Angiogenesis in Patients With Cerebral Ischemic Stroke. Stroke. 1994;25(9):1794-8.

80.   Plate HK. Mechanisms of Angiogenesis in the Brain. Journal of Neuropathology and Experimental Neurology. 1999;58(4):313-20.

81.   Garcia J, Cox J, Hudgins W. Ultrastructure of the microvasculature in experimental cerebral infarction. Acta Neuropathologica. 1971;18(4):273-85.

82.   Gunsilius E, Petzer AL, Stockhammer G, Kähler CM, Gastl G. Serial measurement of vascular endothelial growth factor and transforming growth factor-beta1 in serum of patients with acute ischemic stroke. 2001. p. 275.

83.   Takeshi H, Nobuo N, Taku S, Pak HC. Temporal Profile of Angiogenesis and Expression of Related Genes in the Brain After Ischemia. Journal of Cerebral Blood Flow & Metabolism. 2003;23(2):166.

84.   Del Zoppo JG, Schmid-Schönbein WG, Mori RE, Copeland RB, Chang RC-M. Polymorphonuclear Leukocytes Occlude Capillaries Following Middle Cerebral Artery Occlusion and Reperfusion in Baboons. Stroke. 1991;22(10):1276-83.

85.   Yilmaz G, Granger D. Leukocyte Recruitment and Ischemic Brain Injury. NeuroMolecular Medicine. 2010;12(2):193-204.

86.   Geoffrey B. Purinergic signalling and disorders of the central nervous system. Nature Reviews Drug Discovery. 2008;7(7):575.

87.   Hoek RM, Ruuls SR, Murphy CA, Wright GJ, Goddard R, Zurawski SM, et al. Down-Regulation of the Macrophage Lineage through Interaction with OX2 (CD200). Science. 2000;290(5497):1768-71.

88.   Kleinschnitz C, Schwab N, Kraft P, Hagedorn I, Dreykluft A, Schwarz T, et al. Early detrimental T-cell effects in experimental cerebral ischemia are neither related to adaptive immunity nor thrombus formation. 2010. p. 3835-42.

89.   Arumugam T, Granger D, Mattson M. Stroke and T-cells. Neuromolecular Medicine. 2005;7(3):229-42.

90.   Becker K, Kindrick D, Relton J, Harlan J. Antibody to the alpha4 integrin decreases infarct size in transient focal cerebral ischemia in rats / Editorial comment. Stroke. 2001;32(1):206-11.

91.   Schilling M, Besselmann M, Müller M, Strecker JK, Ringelstein EB, Kiefer R. Predominant phagocytic activity of resident microglia over hematogenous macrophages following transient focal cerebral ischemia: An investigation using green fluorescent protein transgenic bone marrow chimeric mice. Experimental Neurology. 2005;196(2):290-7.

92.   Adam D, Rishma V, Jianghua F, Johanna N, Barry WM, Risto AK, et al. Proliferating resident microglia after focal cerebral ischaemia in mice. Journal of Cerebral Blood Flow & Metabolism. 2007;27(12):1941.

93.   Lalancette-Hébert M, Gowing G, Simard A, Weng YC, Kriz J, Lalancette-Hébert M. Selective ablation of proliferating microglial cells exacerbates ischemic injury in the brain. 2007. p. 2596-605.

94.   Arthur L, Elisabeth S-P, Claudia V, Henrike D, Clemens S, Serge R, et al. Regulatory T cells are key cerebroprotective immunomodulators in acute experimental stroke. Nature Medicine. 2009;15(2):192.

95.   Marler J. Tissue Plasminogen Activator for Acute Ischemic Stroke. The New England Journal of Medicine. 1995;333(24):1581-8.

96.   Wardlaw JM, Murray V, Berge E, Del Zoppo GJ, Wardlaw JM. Thrombolysis for acute ischaemic stroke. 2014. p. CD000213-CD.

97.   Schaller J, Gerber S. The plasmin–antiplasmin system: structural and functional aspects. Cellular and Molecular Life Sciences. 2011;68(5):785-801.

98.   Tissue Plasminogen Activator for Acute Ischemic Stroke. The New England Journal of Medicine. 1995;333(24):1581-8.

99.   Zerna C, Thomalla G, Campbell BCV, Rha J-H, Hill MD. Current practice and future directions in the diagnosis and acute treatment of ischaemic stroke. The Lancet. 2018;392(10154):1247-56.

100.   Filho JO SO. Mechanical thrombectomy for acute ischemic stroke UpToDate2019 [updated 22.03.2019; cited 2019 17.04.]. Available from: https://www.uptodate.com/contents/mechanical-thrombectomy-for-acute-ischemic-stroke?search=endovascular therapy&source=search_result&selectedTitle=1~150&usage_type=default&display_rank=1.

101.   Hacke W, Kaste M, Bluhmki E, Brozman M, Dávalos A, Guidetti D, et al. Thrombolysis with Alteplase 3 to 4.5 Hours after Acute Ischemic Stroke. The New England Journal of Medicine. 2008;359(13):1317-29.

102.   Zhang ZG, Chopp M. Neurorestorative therapies for stroke: underlying mechanisms and translation to the clinic. Lancet Neurology. 2009;8(5):491-500.

103.   Zhang RL, Zhang ZG, Zhang L, Chopp M. Proliferation and differentiation of progenitor cells in the cortex and the subventricular zone in the adult rat after focal cerebral ischemia. Neuroscience. 2001;105(1):33-41.

104.   Katakowski M, Zhang ZG, Chen J, Zhang R, Wang Y, Jiang H, et al. Phosphoinositide 3-kinase promotes adult subventricular neuroblast migration after stroke. 2003. p. 494-501.

105.   Zacharek A, Chen J, Li A, Cui X, Li Y, Roberts C, et al. Angiopoietin1/TIE2 and VEGF/FLK1 Induced by MSC Treatment Amplifies Angiogenesis and Vascular Stabilization after Stroke. Journal of Cerebral Blood Flow & Metabolism. 2007;27(10):1684-91.

106.   Llovera G, Roth S, Plesnila N, Veltkamp R, Liesz A. Modeling Stroke in Mice: Permanent Coagulation of the Distal Middle Cerebral Artery. Journal of Visualized Experiments. 2014(89).

107.   Carmichael S. Rodent models of focal stroke: Size, mechanism, and purpose. NeuroRX. 2005;2(3):396-409.

108.   Watson C, Paxinos G, Puelles L. Vascular Supply. 2012. In: The mouse nervous system [Internet]. Amsterdam: Academic Press. 1st ed.; [459-72].

109.   Canazza A, Minati L, Boffano C, Parati E, Binks S, Canazza A. Experimental models of brain ischemia: a review of techniques, magnetic resonance imaging, and investigational cell-based therapies. Frontiers in neurology. 2014;5:19-.

110.   Pucino V, Bombardieri M, Pitzalis C, Mauro C. Lactate at the crossroads of metabolism, inflammation, and autoimmunity. European Journal of Immunology. 2017;47(1):14-21.

111.   Errea A, Cayet D, Marchetti P, Tang C, Kluza J, Offermanns S, et al. Lactate Inhibits the Pro-Inflammatory Response and Metabolic Reprogramming in Murine Macrophages in a GPR81-Independent Manner.(Research Article). PLoS ONE. 2016;11(11):e0163694.

112.   Mason S, Mason S. Lactate Shuttles in Neuroenergetics-Homeostasis, Allostasis and Beyond. Frontiers in neuroscience. 2017;11:43-.

113.   Ahmed K, Tunaru S, Tang C, Müller M, Gille A, Sassmann A, et al. An Autocrine Lactate Loop Mediates Insulin-Dependent Inhibition of Lipolysis through GPR81. Cell Metabolism. 2010;11(4):311-9.

114.   Dey P. Fixation of Histology Samples: Principles, Methods and Types of Fixatives. Basic and Advanced Laboratory Techniques in Histopathology and Cytology: Singapore: Springer Singapore; 2018. p. 3-17.

115.   Gage GJ, Kipke DR, Shain W. Whole Animal Perfusion Fixation for Rodents. Journal of Visualized Experiments. 2012(65).

116.   Fix AS, Garman RH. Practical Aspects of Neuropathology: A Technical Guide for Working with the Nervous System. Thousand Oaks, CA2000. p. 122-31.
117.   Thavarajah R, Mudimbaimannar V, Elizabeth J, Rao U, Ranganathan K. Chemical and physical basics of routine formaldehyde fixation.(Review Article)(Report). Journal of Oral and Maxillofacial Pathology. 2012;16(3):400.
118.   Dey P. Staining Principle and General Procedure of Staining of the Tissue. Basic and Advanced Laboratory Techniques in Histopathology
and Cytology: Springer; 2018. p. 57-67.
119.   Swanson RA, Morton MT, Tsao-Wu G, Savalos RA, Davidson C, Sharp FR. A semiautomated method for measuring brain infarct volume. Journal of cerebral blood flow and metabolism : official journal of the International Society of Cerebral Blood Flow and Metabolism. 1990;10(2):290-3.
120.   Corthell JT. Immunohistochemistry. Basic Molecular Protocols in Neuroscience: Tips, Tricks, and Pitfalls: Elsevier Science; 2014. p. 91-103.
121.   Kalyuzhny AE. Immunohistochemistry: Essential Elements and Beyond. Cham: Springer International Publishing, Cham; 2016.
122.   Immunocytochemical Methods and Protocols. Totowa, NJ: Humana Press, Totowa, NJ; 2010.
123.   Russell WMS, Burch RL. The principles of humane experimental technique. London: Methuen; 1959.
124.   Perlman RL, Perlman RL. Mouse models of human disease: An evolutionary perspective. Evolution, medicine, and public health. 2016;2016(1):170-6.
125.   Dirk M. Hermann TRD. From Bedside to Bench: How Clinical Reality Should Instruct
Stroke Modeling. In: Dirnagl U, editor. Neuromethods: Rodent Models of Stroke. 47. Totowa, NJ: Humana Press, Totowa, NJ; 2010. p. 1-6.
126.   E L, Lu J, Selfridge JE, Burns JM, Swerdlow RH. Lactate administration reproduces specific brain and liver exercise-related changes. New York2013. p. 91-100.
127.   Lønbro S, Wiggins JM, Wittenborn T, Elming PB, Rice L, Pampo C, et al. Reliability of blood lactate as a measure of exercise intensity in different strains of mice during forced treadmill running. PLOS ONE. 2019;14(5):e0215584.
128.   Sugimori H, Yao H, Ooboshi H, Ibayashi S, Iida M. Krypton laser-induced photothrombotic distal middle cerebral artery occlusion without craniectomy in mice. Brain Research Protocols. 2004;13(3):189-96.
129.   Palay SL, McGee-Russell SM, Gordon S, Grillo MA. Fixation of neural tissues for electron microscopy by perfusion with solutions of osmium tetroxide. The Journal of cell biology. 1962;12:385.
130.   Overgaard K, Meden P. Influence of different fixation procedures on the quantification of infarction and oedema in a rat model of stroke. Neuropathology and Applied Neurobiology. 2000;26(3):243-50.
131.   Dey P. Tissue Microtomy: Principle and Procedure. Basic and Advanced Laboratory Techniques in Histopathology and Cytology: Springer; 2018. p. 41-50.
132.   Bederson JB, Pitts LH, Germano SM, Nishimura MC, Davis RL, Bartkowski HM. Evaluation of 2,3,5-triphenyltetrazolium chloride as a stain for detection and quantification of experimental cerebral infarction in rats. 1986. p. 1304-8.
133.   Spring S, Lerch JP, Wetzel MK, Evans AC, Henkelman RM. Cerebral asymmetries in 12-week-old C57Bl/6J mice measured by magnetic resonance imaging. NeuroImage. 2010;50(2):409-15.
134.   McColl BW, Rothwell NJ, Allan SM, McColl BW. Systemic inflammatory stimulus potentiates the acute phase and CXC chemokine responses to experimental stroke and

exacerbates brain damage via interleukin-1- and neutrophil-dependent mechanisms. The Journal of neuroscience : the official journal of the Society for Neuroscience. 2007;27(16):4403-12.

135.   Wang RY, Lin XJ, Yang GY, Gao PJ, Shen GX. Effect of hirulog-like peptide on middle cerebral artery occlusion-induced brain injury in mice. Neuroscience. 2014;277:568-76.

136.   Lalancette-Hébert M, Gowing G, Simard A, Weng YC, Kriz J, Lalancette-Hébert M. Selective ablation of proliferating microglial cells exacerbates ischemic injury in the brain. The Journal of neuroscience : the official journal of the Society for Neuroscience. 2007;27(10):2596-605.

137.   Schilling M, Strecker JK, Schäbitz WR, Ringelstein EB, Kiefer R. Effects of monocyte chemoattractant protein 1 on blood-borne cell recruitment after transient focal cerebral ischemia in mice. Neuroscience. 2009;161(3):806-12.

138.   Lipman NS, Jackson LR, Trudel LJ, Weis-Garcia F. Monoclonal Versus Polyclonal Antibodies: Distinguishing Characteristics, Applications, and Information Resources. ILAR Journal. 2005;46(3):258-68.

139.   Saper CB. A Guide to the Perplexed on the Specificity of Antibodies. Journal of Histochemistry & Cytochemistry. 2009;57(1):1-5.

140.   Bordeaux J, Welsh A, Agarwal S, Killiam E, Baquero M, Hanna J, et al. Antibody validation. BioTechniques. 2010;48(3):197-209.

141.   El-Brolosy MA, Stainier DYR, El-Brolosy MA. Genetic compensation: A phenomenon in search of mechanisms. PLoS genetics. 2017;13(7):e1006780-e.

142.   Gavrieli Y, Sherman Y, Ben-Sasson SA, Gavrieli Y. Identification of programmed cell death in situ via specific labeling of nuclear DNA fragmentation. The Journal of cell biology. 1992;119(3):493-501.

143.   Darzynkiewicz Z, Galkowski D, Zhao H. Analysis of apoptosis by cytometry using TUNEL assay. Methods. 2008;44(3):250-4.

144.   Zille M, Farr TD, Przesdzing I, Müller J, Sommer C, Dirnagl U, et al. Visualizing Cell Death in Experimental Focal Cerebral Ischemia: Promises, Problems, and Perspectives. Journal of Cerebral Blood Flow & Metabolism. 2012;32(2):213-31.

145.   Freret T, Bouet V, Leconte C, Roussel S, Chazalviel L, Divoux D, et al. Behavioral Deficits After Distal Focal Cerebral Ischemia in Mice: Usefulness of Adhesive Removal Test. Behavioral Neuroscience. 2009;123(1):224-30.

146.   Keller D, Ero C, Markram H. Cell Densities in the Mouse Brain: A Systematic Review.(Report)(Brief article). Frontiers in Neuroanatomy. 2018;12.

147.   Nimmerjahn A, Kirchhoff F, Helmchen F. Resting Microglial Cells Are Highly Dynamic Surveillants of Brain Parenchyma in Vivo. Science. 2005;308(5726):1314-8.

148.   Lawson LJ, Perry VH, Dri P, Gordon S, Lawson LJ. Heterogeneity in the distribution and morphology of microglia in the normal adult mouse brain. Neuroscience. 1990;39(1):151-70.

149.   Steen A-B. Quantitative morphological analyses of the striatum and cerebellum of tenascin-R deficient mice.

150.   Furube E, Kawai S, Inagaki H, Takagi S, Miyata S. Brain Region-dependent Heterogeneity and Dose-dependent Difference in Transient Microglia Population Increase during Lipopolysaccharide-induced Inflammation. Scientific reports. 2018;8(1):2203.

151.   Morrison H, Young K, Qureshi M, Rowe R, Lifshitz J. Quantitative microglia analyses reveal diverse morphologic responses in the rat cortex after diffuse brain injury. London2017. p. 1-12.

152.   Barreto G, Sun X, Xu L, Giffard R. Astrocyte Proliferation Following Stroke in the Mouse Depends on Distance from the Infarct. San Francisco2011. p. e27881.

66

153. Li T, Pang S, Yu Y, Wu X, Guo J, Zhang S, et al. Proliferation of parenchymal microglia is the main source of microgliosis after ischaemic stroke. Brain : a journal of neurology. 2013;136(Pt 12):3578-88.

154. Morrison Helena W, Filosa Jessica A. A quantitative spatiotemporal analysis of microglia morphology during ischemic stroke and reperfusion. Journal of Neuroinflammation. 2013;10(1):4.

155. Patel AR, Ritzel R, McCullough LD, Liu F, Patel AR. Microglia and ischemic stroke: a double-edged sword. International journal of physiology, pathophysiology and pharmacology. 2013;5(2):73-90.